Nanoscale

REVIEW

View Article Online
View Journal | View Issue

Cite this: *Nanoscale*, 2024, **16**, 3243

A comprehensive review on singlet oxygen generation in nanomaterials and conjugated polymers for photodynamic therapy in the treatment of cancer

Neetika Singh, Ria Sen Gupta and Suryasarathi Bose *

A key role in lessening humanity's continuous fight against cancer could be played by photodynamic therapy (PDT), a minimally invasive treatment employed in the medical care of a range of benign disorders and malignancies. Cancerous tissue can be effectively removed by using a light source-excited photosensitizer. Singlet oxygen and reactive oxygen species are produced *via* the photosensitizer as a result of this excitation. In the recent past, researchers have put in tremendous efforts towards developing photosensitizer molecules for photodynamic treatment (PDT) to treat cancer. Conjugated polymers, characterized by their efficient fluorescence, exceptional photostability, and strong light absorption, are currently under scrutiny for their potential applications in cancer detection and treatment through photodynamic and photothermal therapy. Researchers are exploring the versatility of these polymers, utilizing sophisticated chemical synthesis and adaptable polymer structures to create new variants with enhanced capabilities for generating singlet oxygen in photodynamic treatment (PDT). The incorporation of photosensitizers into conjugated polymer nanoparticles has proved to be beneficial, as it improves singlet oxygen formation through effective energy transfer. The evolution of nanotechnology has emerged as an alternative avenue for enhancing the performance of current photosensitizers and overcoming significant challenges in cancer PDT. Various materials, including biocompatible metals, polymers, carbon, silicon, and semiconductor-based nanomaterials, have undergone thorough investigation as potential photosensitizers for cancer PDT. This paper outlines the recent advances in singlet oxygen generation by investigators using an array of materials, including graphene quantum dots (GQDs), gold nanoparticles (Au NPs), silver nanoparticles (Ag NPs), titanium dioxide (TiO_2), ytterbium (Yb) and thulium (Tm) co-doped upconversion nanoparticle cores (Yb/Tm-co-doped UCNP cores), bismuth oxychloride nanoplates and nanosheets (BiOCl nanoplates and nanosheets), and others. It also stresses the synthesis and application of systems such as amphiphilic block copolymer functionalized with folic acid (FA), polyethylene glycol (PEG), poly(β-benzyl-L-aspartate) (PBLA10) (FA-PEG-PBLA10) functionalized with folic acid, tetra(4-hydroxyphenyl)porphyrin (THPP-(PNIPAM-*b*-PMAGA)$_4$), pyrazoline-fused axial silicon phthalocyanine (HY-SiPc), phthalocyanines (HY-ZnPcp, HY-ZnPcnp, and HY-SiPc), silver nanoparticles coated with polyaniline (Ag@PANI), doxorubicin (DOX) and infrared (IR)-responsive poly(2-ethyl-2-oxazoline) (PEtOx) (DOX/PEtOx-IR NPs), particularly in NIR imaging-guided photodynamic therapy (fluorescent and photoacoustic). The study puts forward a comprehensive summary and a convincing justification for the usage of the above-mentioned materials in cancer PDT.

Received 15th November 2023,
Accepted 2nd January 2024

DOI: 10.1039/d3nr05801h

rsc.li/nanoscale

1. Introduction

Cancer is increasingly a global health issue, characterized by uncontrollable cell growth and division. Cancer has become one of the most important health concerns in modern times due to its significant impact on human well-being. Despite enormous efforts, there has been limited success in developing clinical treatments, and fatality rates remain high. The International Agency for Research on Cancer estimates that 10 million malignant tumour deaths and 19.3 million new cancer diagnoses will occur globally in 2020.[1,2] Over the past decade, conventional therapies like chemotherapy, surgery and radiotherapy had a reasonable impact. Chemotherapy is currently the primary and most successful mode of tumor therapy in the clinic.[3] In this context, phototherapies like photodynamic treatment (PDT) and photothermal treatment (PTT)

Department of Materials Engineering, Indian Institute of Science, Bangalore, Karnataka - 560012, India. E-mail: sbose@iisc.ac.in

have visible encouraging outcomes in the treatment of cancer. Treatment methods that integrate laser light with photosensitizers (PSs) provide great spatial-temporal controllability, low invasiveness, and little medication resistance.[4] When a photosynthetic system is photoexcited, its ground state (S0) rapidly transitions to the lowest excited singlet state (S1). Subsequently, as the excited state follows non-radiative pathways, it may decay back to the ground state, potentially generating heat in the process. Notably, irreversible cell necrosis occurs when the temperature reaches 42 °C. Elevated temperatures can expedite cell death through mechanisms like ischemia, vascular thrombosis, and the degradation of cell membranes and proteins. Furthermore, the excited energy of the triplet state can lead to the production of extremely reactive oxygen species (ROS) if the excited state decays back to the triplet state (T1) *via* intersystem crossover (ISC).[5,6] ROS is a collective term representing a family of molecules, and the specific molecular identity of each ROS is crucial for understanding its chemical reactivity and biological responses. Nonetheless, the term ROS remains valuable for providing a general description of downstream phenotypes. Major ROS in living systems encompass superoxide ($[O_2]^{\bullet}$), hydrogen peroxide (H_2O_2), hypochlorous acid (HOCl), singlet oxygen ($^1O_2$), lipid peroxides (ROOH), ozone (O_3), and the hydroxyl radical ($[OH]^{\bullet}$). Determining whether a particular ROS is present at sufficiently high concentrations to engage in productive chemistry in a given scenario is fundamental for comprehending its impact on biology.[7] Singlet oxygen ($^1O_2$) has been shown to oxidize chromogenic substrates when created by photosensitization without H_2O_2 oxidation or enzymes.[8] For the formation of singlet oxygen, a photosensitizer, dissolved molecular oxygen, and a suitable wavelength of light are required.[9] Excitation of photosensitizers should be capable of efficient intersystem crossing, allowing for energy transfer to ground-state molecular oxygen.[10] Singlet oxygen is vital in photodynamic treatment (PDT), which is based on the idea that cancer cells are eliminated by deadly reactive oxygen species (ROS). Treatments for a range of conditions, such as dermatological, ophthalmology, cardiovascular, and oncological conditions, have been addressed with this therapy, which is named as a prospective treatment. PDT uses light, molecules of oxygen, and photosensitizers (PS).[11] This review centres on the latest developments in PDT that target cancer cells. The review also looks at the existing methods and strategies for producing singlet oxygen in PDT as described by other authors.[12] The review concludes with an overview of the work of other authors on the design and development of fluorescent probes, conjugated polymers and their nanoparticles, and fluorescent conjugated polymers used in PDT for singlet oxygen generation.

2. Background and mechanism of singlet oxygen generation

Less stable than molecular oxygen in its electronic ground state, "singlet oxygen" is the electronically excited state in which molecules of oxygen exist (Fig. 1). Two unpaired electrons make up the ground state of molecular oxygen. This is because its HOMO ($^3\sum_g^-$, Fig. 2a) has two degenerate orbitals. Three states arranged vertically in ascending energy sequence are shown in Fig. 2b. In the case of oxygen, the energy of the two excited singlet (electron-coupled) states is 150 kJ mol^{-1} for $^1\sum_g^+$ and 95 kJ mol^{-1} for $^1\Delta_g$.[13,14] The bulk of singlet oxygen photophysicochemical events are identified from the $^1\Delta_g$ state because, under typical experimental circumstances, the $^1\sum_g^+$ (higher excited) state rapidly relaxes to the lower energy $^1\Delta_g$ state. The process of producing singlet oxygen often involves transferring energy from a photosensitizer's excited state to the oxygen molecule (Fig. 2b).[13] Triplet energy transfer ($T1_{,PS}$ $S0_{,PS}$) to triplet oxygen ($T_1{,}O_2$ $S_1{,}O_2$) is a well-organized spin-coupled process that is triggered by photoexcitation of a high ISC rate PS molecule. As a result, singlet oxygen is produced, which is significantly more reactive than other forms of oxygen and capable of redox chemistry and moderate infrared phosphorescence.

When light in the visible spectrum is absorbed by a sensitizer (often a dye molecule), it is stimulated to its first singlet state and then rapidly intersystem crosses to its first triplet

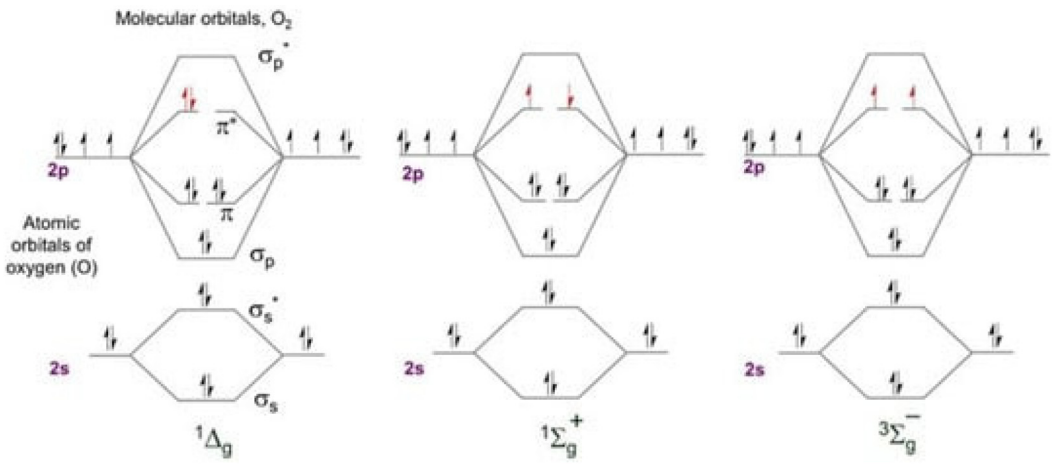

Fig. 1 Molecular orbital energy diagram for the two excited singlet states of oxygen and the triplet ground state.

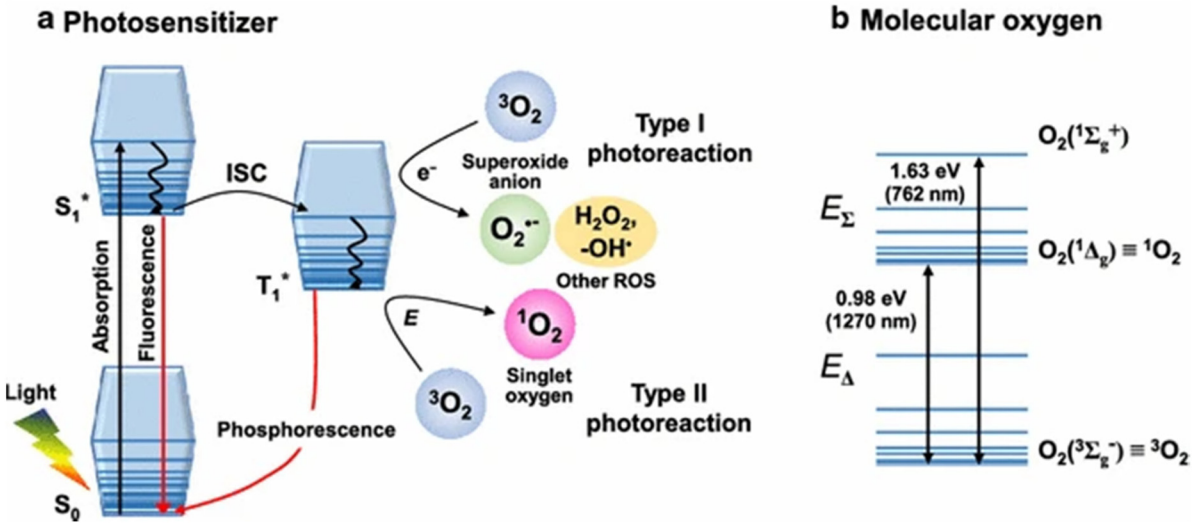

Fig. 2 (a) Jablonski diagram showing the formation of singlet oxygen *via* the transfer of triplet energy from a photosensitizer; (b) relative configuration of molecular oxygen's electronic states.[15]

state (S1, PS T1, PS) in photosensitized singlet oxygen generation (SOG). Spin-coupled triplet energy (T_1, PS S_0, PS)/(T_1,O_2 S_1,O_2) is exchanged between the excited PS and molecular oxygen during this phase. Subsequent developments in laser technology made it possible to directly excite the 3g state to $1g^+$ when excited at 1064 nm, leading to the advent of powerful YAG lasers. Rapid $^3\sum_g^-$, 1g relaxation is the result of the spin-allowed transition (singlet to singlet) and the energy proximity between the two excited states, ruling out any potential physicochemical processes in this species. Conversely, the most effective, useful, and convenient method of producing $^1O_2$ is photosensitized production.[16]

Considering that $^1O_2$ is included in photodynamic therapy (PDT), a newly developed anticancer treatment that combines photoirradiation with photosensitizers (Sens), it is particularly interesting in biological and medical research.[17] In photodynamic therapy (PDT), $^1O_2$ is the first molecule formed under aerobic conditions immediately following photoirradiation. This leads to the direct oxidation of surrounding biomolecules, the shut-down of the circulatory system, and ultimately an immune or inflammatory reaction to cancer tissue. As a result, studying the generation and diffusion dynamics of $^1O_2$ is critical for understanding the anticancer processes of PDT at the molecular level.[18]

Photodynamic therapy (PDT) involves using safe photosensitizing compounds, or photodynamic dyes, in combination with light to achieve a therapeutic effect. These photosensitizers tend to accumulate in cancer tissue. When they are exposed to the appropriate light for their excitation, they become activated when their concentration reaches a specific level. This activation leads to the production of singlet oxygen ($^1O_2$) through a process where an electron from molecular triplet oxygen ($^3O_2$) is transferred to a higher-energy orbital, resulting in a short-lived (fl = 106–109 s) electronically excited state of singlet oxygen (Fig. 3(a)). Singlet oxygen, with a life-

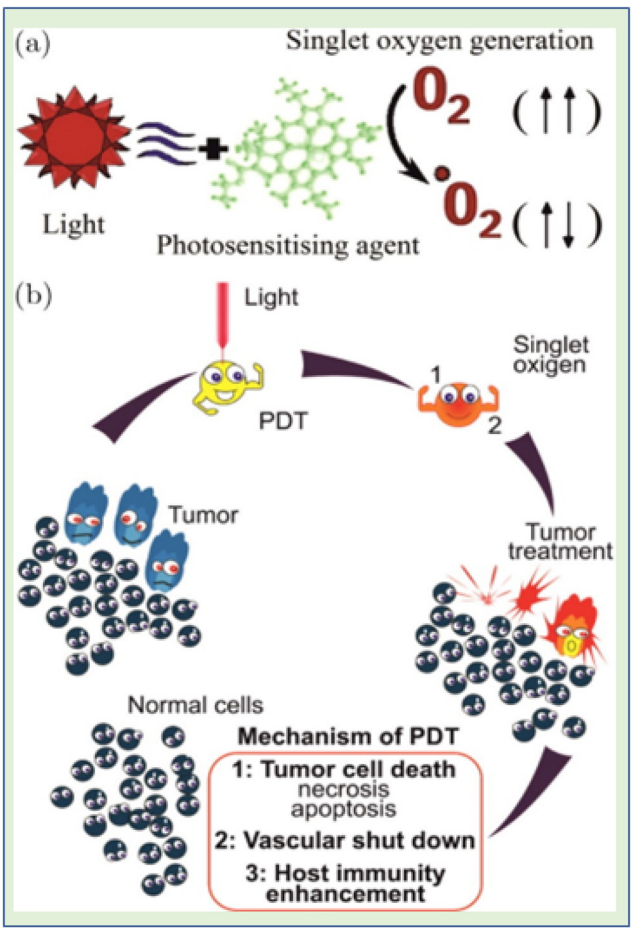

Fig. 3 (a) Electronically excited state (singlet oxygen) in the process of $^1O_2$ production. (b) PDT is regarded as a minimally invasive therapy that targets only tumor cells.[19]

span of only 0.04 to 4 seconds, plays a crucial role in PDT. It can suppress cancer cells by blocking tumor blood vessels and enhancing the host's immune response. This suppression can have either a direct effect, such as necrosis and apoptosis in cancer cells, or an indirect effect, such as the development of blood clots (thrombus). PDT is considered a minimally invasive treatment because it selectively targets cells containing the photosensitizer while sparing the surrounding normal tissues[19] (Fig. 3b).

3. Detection techniques and probes for singlet oxygen generation

Numerous direct and indirect approaches for $^1O_2$ detection have been recognized over the last three decades, as shown in Fig. 4. These techniques can be used in point-spectroscopic or imaging modes.[20]

3.1 Indirect approaches for singlet oxygen generation

Indirect methods for measuring oxygen levels rely on "reporter" or "probe" molecules that change when they interact with oxygen. Various spectroscopic techniques, such as EPR, absorption, fluorescence, and chemiluminescence, are used to detect these changes in the probe's properties. Commercial probes like diphenylisobenzofuran (DPBF), singlet oxygen sensor green (SOSG), fluoresceinyl cypridin luciferin analogue (FCLA), and 2,2,6,6-tetramethylpiperidine (TEMP) are readily accessible and commonly used for these purposes.[21] The benefit is that there is high sensitivity because the "signal" from these probes is quite simple to sense. However, because the lifetimes and therefore diffusion distances of $^1O_2$ in cells and tissue are so tiny, the PS and probe's degree of colocalization at the time of PDT is crucial for producing accurate and understandable data.

One way to lessen the photodynamic effect is to limit the rivalry between the photodynamic reactions of O_2 with the probe and the target cells/tissues. The fact that these probes enable wide-field imaging of $^1O_2$ generation in tumors *in vivo* and quantitative studies of $^1O_2$ generation in homogeneous systems (such as PS solution for comparing different PSs or treatment parameters) makes them still very useful in research settings.

3.2 Direct approaches for singlet oxygen generation

Direct exposure of the NIR luminescence emission of $^1O_2$ at approximately 1270 nm may be considered the "gold standard" for PDT dosimetry;[22] however, due to O_2's enormously high reactivity, which results in a very low emission probability and

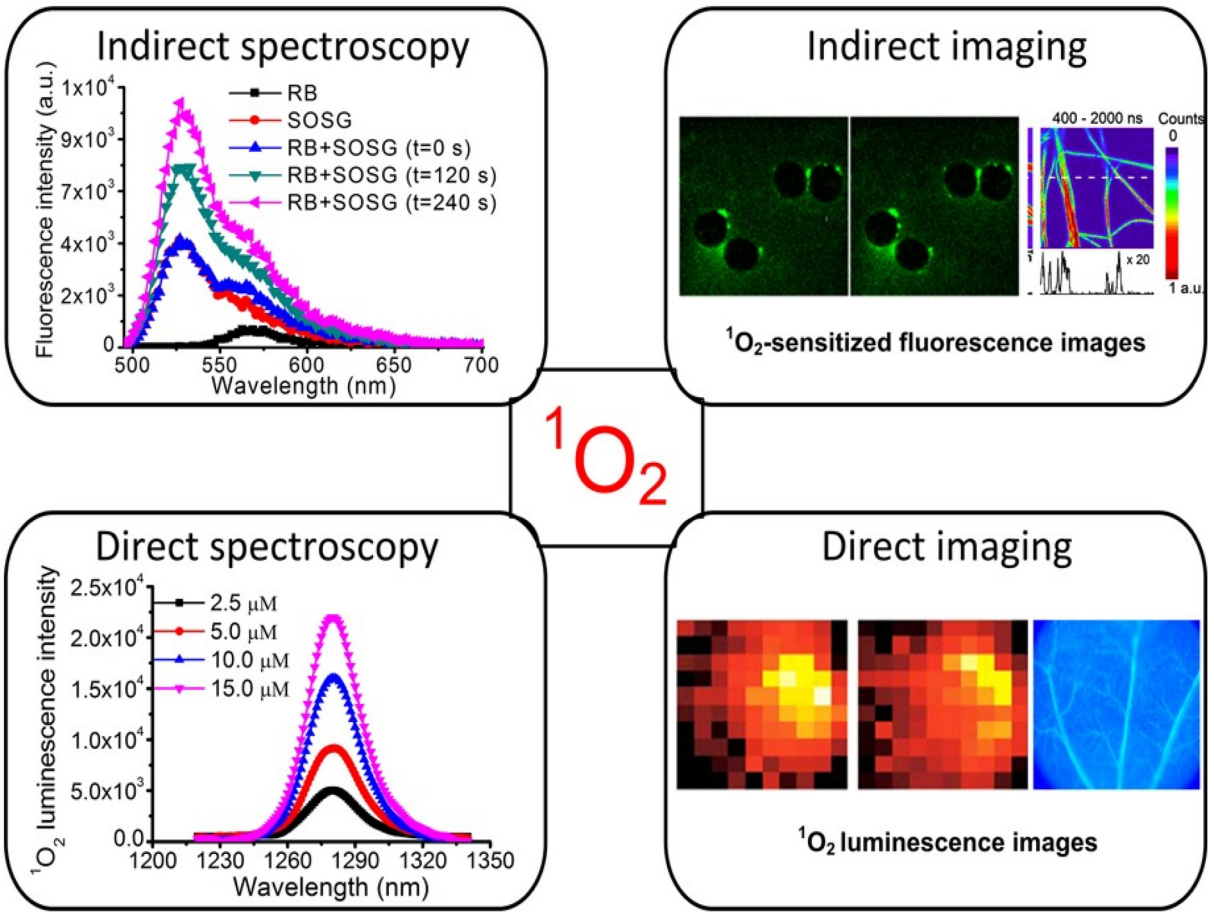

Fig. 4 Methods of $^1O_2$ measurement using both direct and indirect detection.[20]

short lifetime (<1 μs maximum studies) in typical biological microenvironments, there are significant technical tasks. It is extremely faint (1270 emission) because only 1 in 108 $^1O_2$ molecules produce luminescence. The current generation of NIR detectors on the market also do not have particularly high quantum efficiency. Several groups worldwide have developed time and wavelength resolved detection systems that are used to measure $^1O_2$ lifetimes and quantum yields in solution, *in vitro* in cells, and *in vivo* in tissues. High-sensitivity NIR detectors, such as extended-wavelength PMT, short-pulsed (ns) laser sources with high (10 kHz) repetition rates for excitation, and electronics for time-resolved single-photon counting are some of these innovations.[23–26]

Fig. 5 displays a common system architecture for $^1O_2$ luminescence detection with time and wavelength resolution. The excitation light source used to observe the time-resolved $^1O_2$ luminescence was a pulse laser. A filter wheel can be used to hold different BP filters (such as 1190, 1230, 1270, 1310, and 1350 nm) in order to provide wavelength-resolved $^1O_2$ luminescence observations with better collection efficiency. This is in contrast to the spectral discrimination that a monochromator provides. For the purpose of measuring and counting the NIR luminescence, the best commercial PMT (H10330-45, Hamamatsu, Japan) and the fastest photon counter (MSA-300 multichannel, Becker & Hickl GmbH, Germany) were used.[27]

Numerous additional techniques for singlet oxygen ($^1O_2$) detection are based on an examination of the interaction between singlet oxygen molecules and a component that is susceptible to the chemical. Different spectroscopic methods, such as NMR, EPR, UV-vis absorption, or fluorescence, can be used to monitor the change in a sensor molecule's structure, depending on the precise nature of the interaction.[28]

Several probes have been employed for singlet oxygen generation.

Some of the prominent ones include:

3.3 Spectrophotometric probes for singlet oxygen generation

An easier method for finding excited oxygen molecules is spectrophotometry. Singlet oxygen is typically trapped using a chemical probe, after which identification and quantification can be accomplished using an absorbance measurement (Fig. 6).

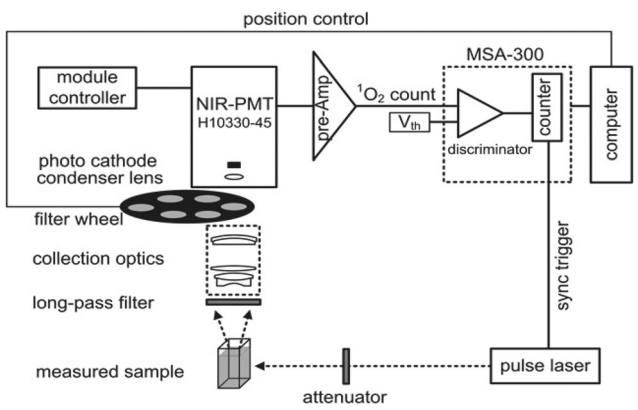

Fig. 5 Schematic diagram of the time- and wavelength-resolved $^1O_2$ luminescence detection system.[20]

3.3.1 9,10-Anthracenedipropionic acid (ADPA). Anthracenedipropionic acid (ADPA), which may be seen by fluorescence and/or absorption spectroscopy,[34] reacts with $^1O_2$ very quickly (reactive rate constant, $k_r = 8 \times 10^7$ m^{-1} s^{-1} in heavy water).[35] ADPA exhibits structured fluorescence and absorption spectra, with maxima at wavelengths of 430 nm and 380 nm, respectively[36] (Fig. 7). Its distinctive absorption/fluorescence is bleached as a result of the interaction with $^1O_2$ and the formation of an endoperoxide adduct.[37] In order to detect singlet oxygen, Wang *et al.* developed BODIPY-doped silica nanoparticles and employed 9,10-anthracenedipropionic acid (ADPA) as a detection agent.[38]

3.3.2 9,10-Dimethyl anthracene (DMA). 9,10-Dimethyl anthracene (DMA), a different anthracene derivative, interacts practically irreversibly with $^1O_2$ in a variety of organic and aqueous media with a very high-rate constant (6.8×10^7–5.7×10^{10} M^{-1} s^{-1}) to produce non-fluorescent 9,10-endoperoxide. In a study by Albiter *et al.*, the development of singlet oxygen ($^1O_2$) from dyes trapped on silica was examined utilizing the photosensitized oxidation of 9,10-dimethyl anthracene (DMA).[39] The same research team studied 9,10-dimethyl anthracene photosensitized oxidation with singlet oxygen in acetonitrile by employing a safranin O/silica composite as a heterogeneous photosensitizer delivery approach[40] (Fig. 8).

3.3.3 9,10-Diphenylanthracene (DPA). 9,10-Diphenylanthracene (DPA) is formed by introducing two phenyl groups at positions 9 and 10 of anthracene. DPA is recognized as a stable and precise singlet oxygen ($^1O_2$) trap with improved endoperoxide stability. However, its detection method relies on a decrease in absorbance at the 355 nm wavelength, which has limitations. DPA is widely acknowledged as a prominent spectrophotometric probe due to its ability to selectively interact with singlet oxygen, resulting in the formation of a stable endoperoxide with a high reaction constant of 1.3×10^6 L mol^{-1}. The rate at which singlet oxygen is produced in the system under investigation is directly proportional to the decline in absorbance at 355 nm. In a notable study conducted by Burguete *et al.*, a benchmark reaction was carried out to investigate singlet oxygen-driven oxidation of DPA. This investigation utilized rose bengal (RB) in various forms, including solution, gel-type generated polymer, and porous monolithic polymer (PMP). The successful application of photodynamic treatment (PDT) of melanoma cells was achieved by enhancing the photoreactivity of PMP–rose bengal conjugates. In summary, DPA is an important compound for singlet oxygen detection and has found application in PDT for melanoma, especially when combined with rose bengal in a PMP configuration[41] (Fig. 9).

3.4 Fluorescence probes for singlet oxygen generation

Since the detection of DPA derivatives depends on the measurement of absorbance, they are not very sensitive as probes. As a result, we created brand-new fluorometric probes

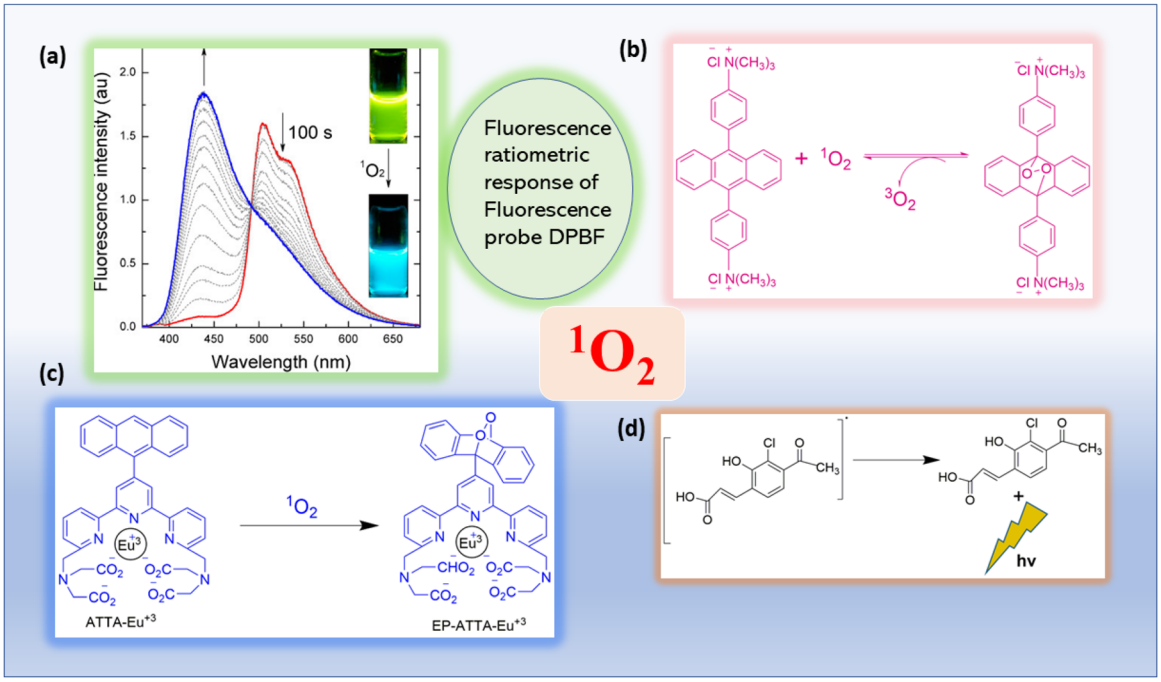

Fig. 6 Absorbance or luminescence-based photophysical singlet oxygen detection methods are illustrated.[29] (a) The inset image displays the fluorescence emission. Reproduced with permission.[30] Copyright 2013, American Chemical Society. (b) UV–Vis absorption based spectrophotometric probe (bis-9,10-anthracene-(4-trimethylphenylammonium) dichloride). Adapted from ref. 31. (c) Reaction of ATTA-Eu^{3+} with $^1O_2$. Adapted from ref. 32. (d) The mechanism of action of the $^1O_2$ chemiluminescent probe SOCL upon interaction with $^1O_2$ and its chemiexcitation route. Adapted from ref. 33.

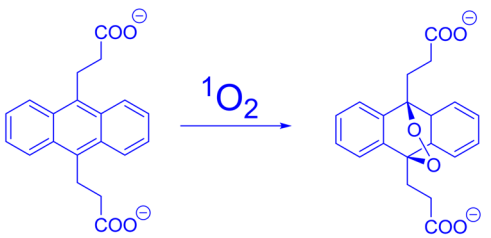

Fig. 7 ADPA's reactivity in the presence of $^1O_2$. Reproduced with permission.[36] Copyright 2016, Elsevier.

for $^1O_2$ to increase sensitivity. Fluorescence measurement is typically more sensitive and is therefore simpler to utilize in imaging research.

3.4.1 1,3-Diphenylisobenzofuran (DPBF). A better alternative could be the chemical 1,3-diphenylisobenzofuran (DPBF). It is excited at 415 nm and shows strong fluorescence; its intensity decreases as it combines with singlet oxygen.[42] To evaluate singlet-oxygen generation efficacy in photosensitized systems, DPBF was employed as the probe.[43] Since other experiments have also indicated that DPBF is a potential choice for superoxide-anion-radical detection, the specificity of DPBF for singlet-oxygen detection is suspicious.[44] Molecular Probes and Invitrogen recently released singlet oxygen sensor green (SOSG), a selective fluorescence sensor, onto the commercial market. Green is the result of the reaction between singlet oxygen and the SOSG fluorescence, which is basically pale blue. Its use in photosensitization systems may be complicated by the fact that the reagent can act as a photosensitizer when exposed to light.[44]

The probe was stated to have a good selectivity for singlet oxygen because its response to hydroxyl radicals or superoxide was minimal.[45] He *et al.* generated singlet oxygen *via* DPBF by using their developed multidipyridylanthracene-bridged organoplatinum(II) metallacycle[46] (Fig. 10).

Phenazine and phenazine-containing photosensitizers **KI-1** to **KI-5** with varying functional groups were fabricated by Imato *et al.* They investigated their photophysical characteristics and photosensitizing potential in order to generate $^1O_2$ using the trapping agent DPBF. By employing DPBF and homochromatic light (509 nm, 300 W cm^2) or constant light (>510 nm, 30 mW cm^2) in THF (air-saturated), the photosensitizing capacity of phenazine derivative **KI-6** was evaluated. Formyl groups were nearly totally changed to hydroxyl groups *via* $NaBH_4$. This was done to demonstrate that phenazine derivatives have superior photosensitizing properties (Fig. 11). The lowering caused the reaction rate (k_{obs}) to drop from 0.144 to 0.009 min^{-1} and the **KI-2** value to drop substantially from 0.48 to 0.05. As a result, formyl groups significantly increase the $^1O_2$ generation of phenazine-based photosensitizers.[47]

3.4.2 9-[2-(3-Carboxy-9,10-diphenyl)anthryl]-6-hydroxy-3*H*-xanthen-3-one (DPAX). A collection of fluorescent probes, 9-[2-(3-carboxy-9,10-diphenyl)anthryl]-6-hydroxy-3*H*-xanthen-3-ones (DPAXs), were recently designed for $^1O_2$ by Tanaka *et al.* DPAXs were the first chemical $^1O_2$ traps that permitted fluorescence

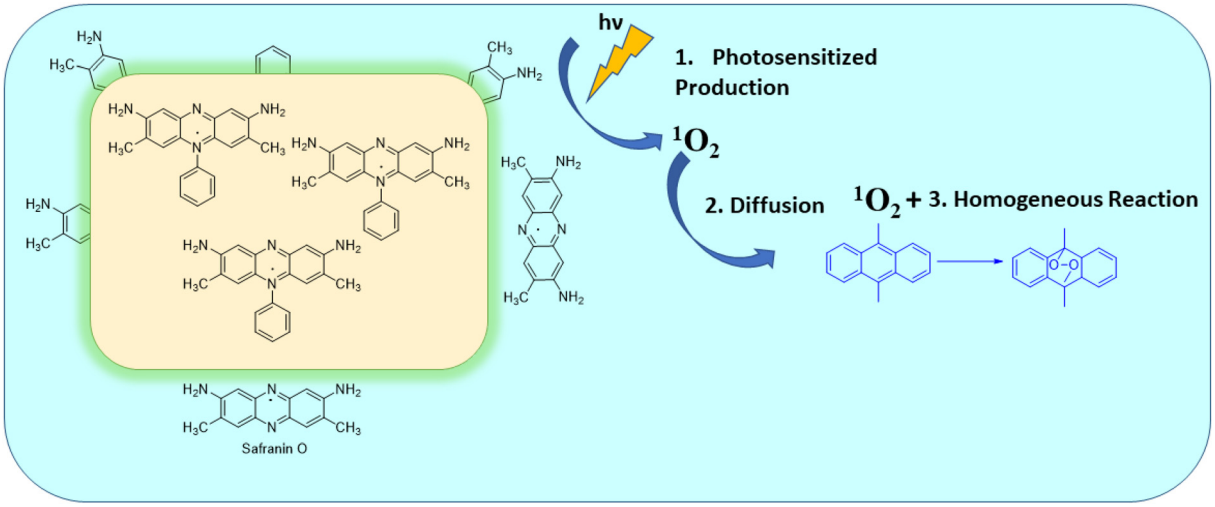

Fig. 8 Schematic representation of the photosensitized oxidation of DMA using SF/SiO_2 composite. This image was taken from ref. 40.

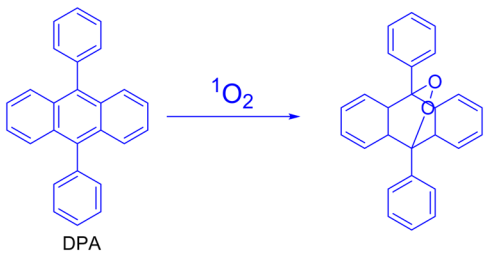

Fig. 9 Singlet oxygen oxidation of DPA to its endoperoxide (*this scheme was taken from* ref. 41).

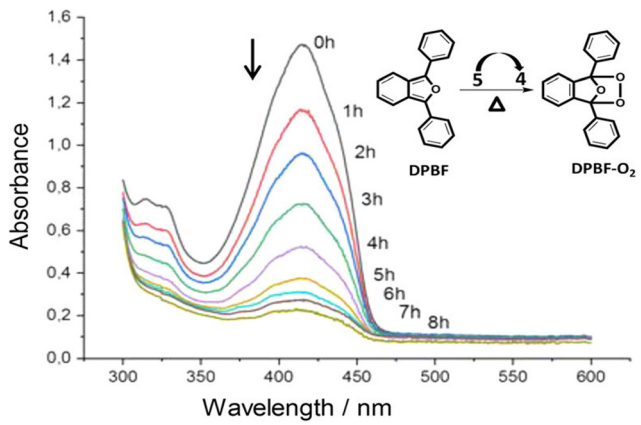

Fig. 10 $^1O_2$ produced by thermolyzing M-EPO reacts with DPBF. Reproduced with permission.[46] Copyright 2020, American Chemical Society.

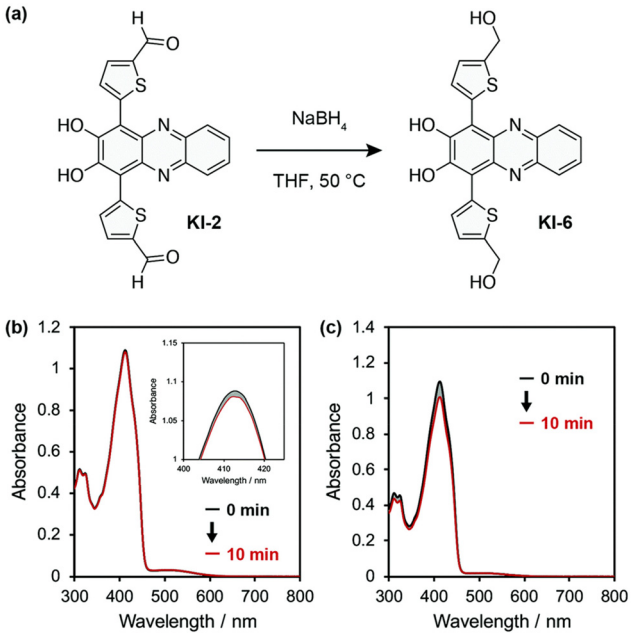

Fig. 11 (a) **KI-6** is created by reducing the formyl groups in the phenazine photosensitizer **KI-2**. (b) After exposure to monochromatic light (509 nm, 300 μW cm^{-2}) in THF, the photoabsorption spectra of DPBF (Abs.@413 nm = *ca.* 1) are recorded in the presence of **KI-6** (Abs. @509 nm = *ca.* 0.03). Magnified image of the peaks at 410 nm is shown in the inset. (c) DPBF (50 μM) photoabsorption spectra with **KI-6** (5 μM) after continuous light exposure (>510 nm, 30 mW cm^{-2}) in THF.[47]

exposure. When they react with $^1O_2$, DPAX endoperoxides (DPAX-EPs) are produced. While DPAXs are derivatives of fluorescein, their fluorescence is significantly less than that of DPAX-EPs.[48] The endoperoxides (DPAX-EPs) exhibit high fluorescence with 0.5–0.7 quantum yield. Nitric oxide, hydrogen peroxide, or superoxide reactions did not modify the fluorescence intensity, demonstrating the strong singlet oxygen specificity of these reactions.[49]

3.4.3 9-[2-(3-Carboxy-9,10-dimethyl) anthryl]-6-hydroxy-3*H*-xanthen-3-one (DMAX). A compound known as 9-[2-(3-carboxy-9,10-dimethyl) anthryl]-6-hydroxy-3*H*-xanthen-3-one, often referred to as DMAX, has been proposed as a tool for detecting singlet oxygen. Unlike its endoperoxide form, DMAX exhibits fluorescence, making it a promising candidate for singlet

oxygen detection, particularly in biological models. DMAX offers several advantages, including being less hydrophobic and more sensitive compared to DPAX, with DMAX being 53 times more sensitive than DPAX. The research conducted by Tanaka *et al.* led to the development of DMAX as a highly sensitive singlet oxygen probe, where the 9,10-dimethylanthracene moiety in this probe acts as a rapid chemical trap for singlet oxygen. DMAX is not known to fluoresce significantly, but its endoperoxide form, DMAX-EP, does exhibit substantial fluorescence, which aligns with predictions from PM3 simulations. In contrast, a class of fluorescent probes for singlet oxygen called 9-[2-(3-carboxy-9,10-diphenyl)-anthryl]-6-hydroxy-3*H*-xanthen-3-ones (DPAXs), developed more recently, are 53 times less sensitive than DMAX and react with singlet oxygen at a faster rate. Consequently, DMAX, as a fluorescence probe, holds promise for detecting singlet oxygen in various biological systems.[50]

3.5 Luminescence probes for singlet oxygen generation

Song and colleagues developed a novel europium(III) complex, [4′-(9-methyl-10-anthryl)-2,2′:6′,2′terpyridine-6,6″-diyl] bis (methylenenitrilo) tetrakis(acetate)Eu^{3+}, with the purpose of serving as a highly precise and targeted time-gated luminescence sensor for singlet oxygen ($^1O_2$). This new probe exhibits exceptional selectivity in reacting with $^1O_2$ to form its endoperoxide (EP-MTTAEu^{3+}) at an impressive rate of 10^{10} M^{-1} s^{-1}. The reaction also results in notable enhancements in both luminescence lifetime (increasing from 0.80 to 1.29 ms) and luminescence quantum yield (rising from 0.90% to 13.8%). This probe demonstrates versatility by functioning effectively over a broad pH range spanning from 3 to 10 and exhibits remarkable water solubility. Furthermore, it boasts a significant stability constant of approximately ~10^{21}, making it a valuable tool for studying singlet oxygen in various research applications[51] (Fig. 12).

3.6 Chemiluminescence probes for singlet oxygen generation

Chemiluminescence is considered one of the most effective methods for detecting singlet oxygen. Unlike fluorescence, chemiluminescence does not require an excitation light source, which eliminates issues related to background fluorescence and scattered light interference. This approach also reduces the risk of UV irradiation causing harm to living cells during fluorescence measurements while enhancing the signal-to-noise ratio. In recent years, the pursuit of singlet oxygen detection has led to the development of various chemiluminescence sensors. Among them, the most commonly used chemiluminescence probes for singlet oxygen include 2-methyl-6-phenyl-3,7-dihydroimidazo [1,2-*a*] pyrazin-3-one (CLA) and its derivatives, namely MCLA and FCLA (Fig. 13a–c). These compounds emit light on their own in the presence of singlet oxygen, making them valuable tools for singlet oxygen detection.[52,53]

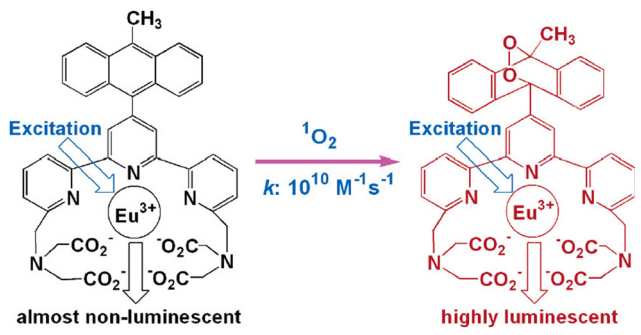

Fig. 12 Reaction of MTTA–Eu^{3++} with $^1O_2$. Reproduced with permission.[51] Copyright 2006, American Chemical Society.

4. Nanomaterials for singlet oxygen generation in PDT

Photodynamic therapy (PDT) has been instrumental towards the effective treatment of certain types of cancer. However, to date its true potential has not been explored clinically owing to several practical bottlenecks such as the dearth of photosensitizers (PSs) with high selectivity towards tumors, efficiency in ROS generation, *etc*.

Although PSs with porphyrin structures, natural products and synthetic dyes have shown clinical applicability, inherent deficiencies including poor levels of water solubility, diminished cancer cell selectivity, ineffective photostability and $^1O_2$ quantum yield, still pose major roadblocks.[54–56]

A quantum leap in terms of performance advancement of PDT has been achieved in the recent past due to technical advancements in the field of nanotechnology. Candidates including but not limited to carbon, metal and polymer nanomaterials have been dynamically established as nanomaterial-based PSs. Herein, we summarize how a wide range of nano-PSs with enhanced and distinctive photodynamic as well as photochemical properties can be deployed for augmenting singlet oxygen generation efficacy. This in turn can be further extrapolated for usage in PDT.

4.1 Metal-based nanoparticles

Recent studies suggest the possibility of directly sensitizing metal-based nanomaterials (NMs) for the generation of extremely cytotoxic $^1O_2$. They act as a potential and viable tool for observing the therapeutic efficacy of PDT.

Amongst the metal NMs, Au NMs have garnered immense research interest compared to other metal nanoparticles. Their ultrahigh chemical inertness, immense biocompatibility, tailorable optical characteristics, easy and tunable surface modifications and huge extinction coefficients make them versatile and potential candidates for PDT. Strong localized surface plasmon resonance features enable easy light absorption and subsequently generate heat, leading to effective photothermal characteristics. Additionally, their ability to be directly sensitized for SOG have also helped them to carve out a niche for themselves.

In line with cancer PDT, Au NPs stabilized *via* chemicals were found to be extremely effective at SOG. Several studies

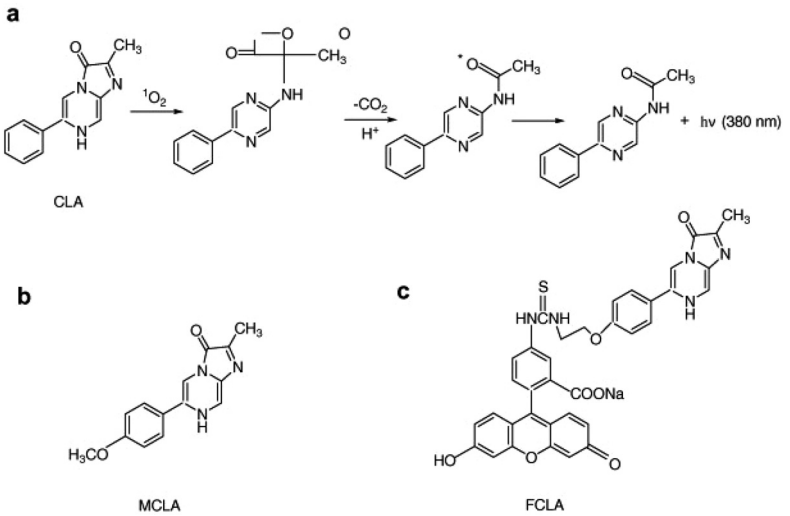

Fig. 13 (a) Chemical structure of CLA and its reaction mechanism with singlet oxygen. Chemical structures of (b) FCLA and (c) MCLA. Reproduced with permission.[49] Copyright 2010, Elsevier.

have reported the efficacy of chemically conjugating and modifying Au NPs for such treatment procedures. Chadwick *et al.* reported citrate stabilized Au NPs for SOG.[57] The photogeneration process was actuated *via* laser irradiation, which was pulsed, and the operation progressed *via* equilibrated hot electrons. They also corroborated the fact that the size of Au NPs had a profound effect on the efficiency of SOG. Following this, Gao *et al.* fabricated DNA-driven shell–satellite Au–Ag plasmonic NPs for PDT. The fabricated assemblies exhibited chiroplasmonic features in the visible range. Additionally, very high ROS generation efficacy was reported for the synthesized particles.[58] Gold NPs conjugated with pectin and folic acid were synthesized *via* a facile chemical reduction method by Kumari *et al.* Pectin was meant to be a stabilizer and folic acid functioned as an effective cancer cell receptor.[59] The presence of the folic acid component helped in the development of conjugations inside and outside the pectin matrix on top of the Au NP surface which in turn augmented the generation of $^1O_2$. Similarly, Au NCs stabilised by 11-mercaptoundecanoic acid were reported by Hwang and his group in 2015.[60] These NCs (nanoclusters) were conjugated with TAT-peptide to form nucleus targeting NCs. Gene transfection exhibited *via* these nanomaterials was about 81% in HeLa cells and TAT-Au NCs could sensitize SOG, which in turn augments intracellular ROS and causes cell death. Kawasaki and Miyata *et al.* worked along similar lines where they stabilized Au NCs with thiol and captotil.[61,62] The synthesized Au NCs could emit red fluorescence and sensitize SOG. Such generation efficiency could effectively cause the death of cancer and microbial cells.

Architecture variation of the Au NPs also affected their SOG efficiency. Chan *et al.* developed core–shell structures with mesoporous silica shells which were coated with gold NRs (AuNR@mS). The fabrication was actuated by the seed crystal growth method. Herein ROS generation was affected by integrating Merocyanine 540 PS in the mesoporous silica core. The surface plasma resonance effect of Au NRs further augmented ROS production.[63] Along similar lines, Farooq *et al.* optimized a nanoshell architecture with an Au shell and silica core for maximizing SOG efficiency *via* deploying a methylene blue (MB) PS.[64] The presence of gold nanoshells greatly enhanced SOG in MB solutions by a huge margin of 320%.

Apart from core–shell architectures, Au NPs were often reported in other forms too. For example, Au nanorods, another form of Au NP, were researched by several scientists across the globe. Au NRs coated with PVP (polyvinylpyrrolidone) were reported by Zhao *et al.* Here, the NRs could be precisely sensitized for SOG *via* two-photon excitation (TPE).[65] They varied the aspect ratios of the fabricated NRs and it was found that all the NRs facilitated the absorption of TPE for oxygen sensitization. It was observed that the fabricated Au NRs could effectively kill nearly 85% of HeLa cells. The same group later demonstrated the fact that the efficacy of TPE induced singlet oxygen generation could be further enhanced for aggregated NRs.[66]

Along similar lines, Au NRs, when coated with Lipofectamine 2000 (cationic lipid), were found to produce $^1O_2$ when irradiated with a long wavelength of NIR light.[67] Within a period of a few years, the same group led by Vankayala reported a new gold NP architecture, *i.e.* nano-echinus (Au NE). The seed growth technique using the surfactant double-chain cetyltrimethylammonium bromide was used to realise NP formation.[68] The particles were formed with a hydrated radius of 350 ± 50 nm. It was meant to act as a dual nanomaterial in the second biological window for both PDT and PTT.

Besides, core–shell, NRs, and NEs, a new class of Au NP structure, *i.e.* nanocluster (NC), was delineated by many research groups. For example, polyvinyl acetate films impregnated with $HAuCl_4$ and a radical precursor were duly irradiated with UV light for the preparation of Au nanoclusters (NCs).[69] Single-molecule fluorescence spectroscopy (SMS) was

employed to reveal the material's photoreactivity for the first time. The fabricated Au NCs were found to possess tailorable photochemical attributes which were beneficial for PDT. Spin multiplicity and the size of the NC were found to be major contributing factors towards the photochemical activity of the NCs.

With this idea in mind, Das *et al.* established the fact that the fluorescence intensity was greatly affected by the orientation of the oxygen moieties which got adsorbed onto the Au NC surface of different sizes.[70] Au NCs of smaller sizes stabilized with BSA protein molecules had a superoxo orientation of oxygen, which in turn enhanced the formation of SOG in the presence of O_2.

Hybrid types of NPs with Au were also explored by researchers. Saito *et al.* were amongst the first to detect O^{2-} (superoxide) radicals and $^1O_2$ on Au NP-desposited-TiO_2. The samples were prepared by using 13 commercially available powders of TiO_2 and subsequently SOG and superoxide radical generation were detected[71] (Fig. 14). Due to the mixed crystalline phase effect of TiO_2, such high generation efficiencies were observed and Zhou *et al.* reported the synthesis of Au (gold) nanorod/ZnO (zinc oxide) nanostructures. The nanoparticles were synthesized with different ZnO shell thicknesses. The hybrid structure was found to exhibit enhanced SOG efficacy when compared to Au nanorods or ZnO nanoparticles. The core–shell architecture was helpful at preventing the contact of Au nanoparticles with cell lines, thus reducing cytotoxicity. The SOG efficiency was found to scale linearly with the thickness of ZnO shells.[72]

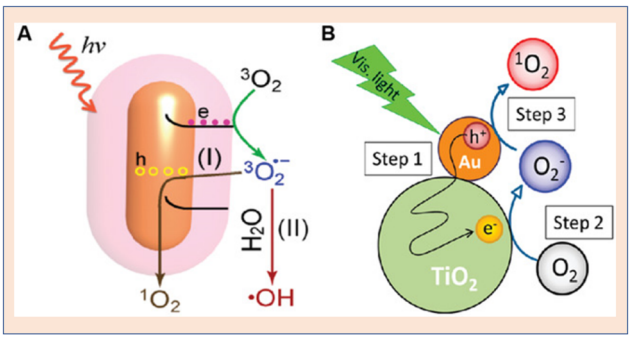

Fig. 14 Schematic representation of singlet oxygen generation from gold nanoparticles. (A) Au nanorod. Reproduced with permission.[73] Copyright 2014, Royal Society of Chemistry. (B) Au NP–TiO_2 core–shell architecture for enhanced SOG. Reproduced with permission.[71] Copyright 2014, American Chemical Society.

It was Pasparakis *et al.* who used a continuous wave laser as well as pulsed laser sources and studied their respective effects on SOG from Au NPs.[74] The pulsed laser was found to be more efficient at SOG. This visible difference was probably due to the different mechanistic pathways taken in sensitizing oxygen by Au NP irradiation.

Mostly Au NPs have been well reported and studied in the literature for their SOG efficacy. However, the exploration of Ag (silver) NPs for controlling SOG is still in its infancy and one of the major roadblocks in their applicability is posed by the troublesome reduction of Ag^+ to Ag and the reduced stability of the NPs in an ambient environment.

Nevertheless, a novel yet facile approach was reported by Yu *et al.* for the fabrication of BSA-templated radically small Au NCs which demonstrated enhanced efficiency at SOG for PDT.[75]

On similar grounds, Aiello *et al.* prepared pectin coated silver-coated NPs and used riboflavin (Rb) as a sensitizer.[76] This led to enhanced SOG, and the superoxide radical significantly contributed to PDT (Fig. 15a). Similarly, in 2016, it was Yu's group who reported a facile synthetic pathway for fabricating BSA-templated Ag nanoclusters which were ultrasmall in size.[75] The Ag NCs exhibited enhanced SOG for treating cancer cells *via* PDT (Fig. 15b).

4.2 Ceramic, metal oxide, and metal-sulfide-based nanoparticles

Ceramic-based NPs including metal oxide NPs have advantageous factors such as particle size, porosity, shape and easy tunable mono-dispersibility.[78–80] These NPs are mostly water soluble and are highly biocompatible in nature. They are

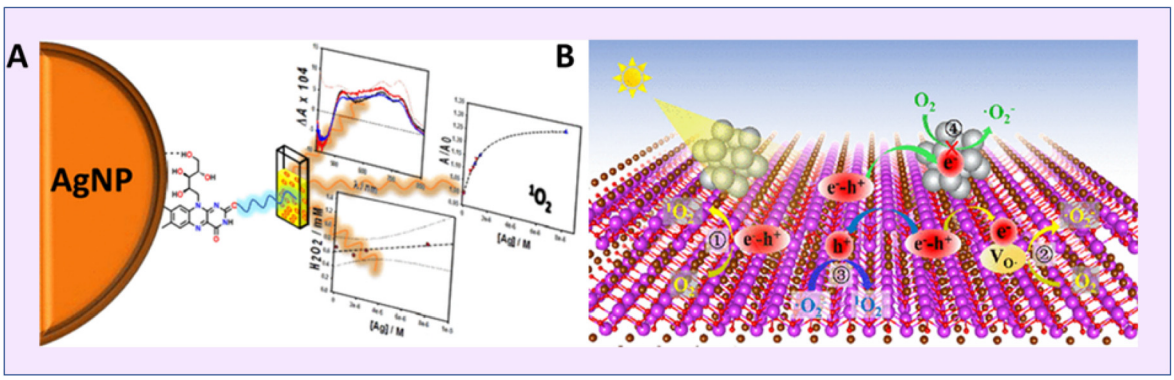

Fig. 15 Schematic representation of singlet oxygen generation from silver nanoparticles. (A) Pectin-stabilized Ag NP. Reproduced with permission.[76] Copyright 2016, American Chemical Society. (B) Defect-free Au NP from FL-BiOBr-NS for enhanced SOG. Reproduced with permission.[77] Copyright 2022, American Chemical Society.

reported to be resistant towards microbial attack and their inherent characteristics such as swelling or porosity are independent of changes in pH.

In this area ground-breaking research was conducted by Prasad and his group, who synthesized silica-based NPs with a diameter of 30 nm. These particles were entrapped within a PS-enabled anticancer drug.[81] The SOG efficiency of these particles was found to be extremely high upon irradiation with light of 532 and 650 nm.

TiO_2 is deemed to be extremely photostable and biocompatible. Such characteristics make it an ideal candidate to be NPs for PDT. Nosaka and his team reported SOG from titanium dioxide NPs in 2004.[82] SOG was facilitated *via* laser irradiation in pulse mode using the gated photon counting method. The augmented photocatalytic oxidation of oxygen at the surface of the NPs was presumed to be the mechanism behind such efficient singlet oxygen generation (SOG).

From the perspective of cancer treatment, it was understood that NIR rays (650–1300 nm) had greater penetration depth inside tissues when compared to the usual UV irradiation. Hence it was thought that the basic integration of a light transducer into the fabricated TiO_2 NPs would convert NIR into UV and hence would prove extremely beneficial for *in vivo* PDT.[83] With this idea in mind, upconversion NPs or UCNPs have gained huge impetus for being incorporated into TiO_2 NPs for treating tumors which are deep seated.

To explore UCNPs, Zhang *et al.* designed a nanocomposite consisting of UCNP–TiO_2 core–shell type particles. A UCNP core was coated with a homogeneous layer of TiO_2[84] (Fig. 16b). With 980 nm laser excitation, the fabricated UCNP could convert the laser source wavelength to UV and visible light, which in turn would activate the TiO_2 layer for the production of reactive oxygen species. With the ability to kill nearly 50% of oral squamous carcinoma cells, these NPs emerged as potential candidates for cancer PDT.

Along similar lines, Wu and his team fabricated composites decorated with folic acid and the composites were abbreviated as FA-Gd-Si-Ti based nanocomposites.[85] Such systems were designed for dual application of MRI (magnetic resonance imaging) and PDT. The presence of folic acid helped in selective binding at folate-based receptors on the cancerous cells thus helping the NPs to gain smooth entry into the cells. With this, 88.6% reduction in the growth inhibition ratio was observed for the tumors. Analogous NPs were synthesized by Lin and his group termed the nanocomposites as (($NaYF_4$:Yb^{3+},Tm^{3+}@$NaGdF_4$:Yb^{3+})@TiO_2). These NPs were to be used for imaging *in vivo* cancer PDT.[86] The hydrophilic PVP polymer assisted protocol was adopted for coating anatase grade titanium dioxide on top of the Yb/Tm-co-doped cores of the UCNPs. Endocytosis was the main mechanism for the take up of NPs by the cancer cells. This would subsequently produce ROS and lead to cell apoptosis.

Although TiO_2 is the major focus for metal oxide-based NPs, tungsten and bismuth oxyhalide (BiOCl) have also been explored by researchers. Tungsten oxide nanowires (NWs) were reported for cancer PDT by Hwang *et al.* PEGylated $W_{18}O_{49}$ NWs were synthesized which could absorb in the NIR region (up to 1200 nm)[87] (Fig. 16c). SOG *via* these nanoparticles was

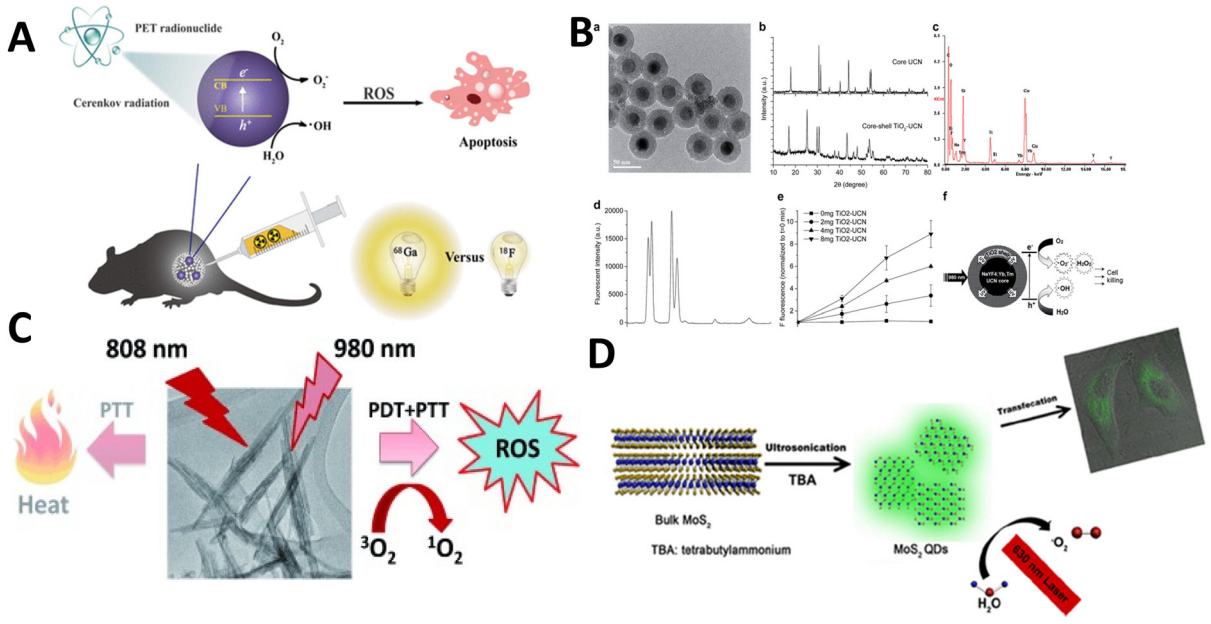

Fig. 16 (A) Activated TiO_2 NPs for PDT. Reproduced with permission.[89] Copyright 2018, American Chemical Society. (B) Titania coated core-shell upconversion NPs and its suitable characterizations (a–f).[84] Copyright 2014, Royal Society of Chemistry. (C) Photodynamic therapeutic nature of PEGylated W18O49 Nanowires. Reproduced with permission.[87] Copyright 2013, Wiley Online Library. (D) Metal sulphide (MoS_2) quantum dots for PDT. Reproduced with permission.[90] Copyright 2016, American Chemical Society.

exemplary when irradiated with 980 nm NIR light. ROS levels were found to be elevated inside HeLa cells when treated with such NPs.

BiOCl possesses a tailorable band gap which facilitates its usage as an emerging photocatalyst that can be well exploited for PDT. Xu *et al.* prepared BiOCl nanoplates and nanosheets *via* a hydrothermal technique and functionalized them with PEI.[88] These NPs were found to significantly reduce MCF cell viability: 70% and 35% for nanosheets and 35% for nanoplates. Their unique morphological features combined with their intrinsic band gaps were responsible for such efficient PDT performance.

Metal sulphide based NPs also contributed to the generation of reactive oxygen species. MOS_2 quantum dots were synthesized through a sonication approach based on a tetrabutylammonium-assisted procedure[90] (Fig. 16d). When irradiated with 630 nm light, the fabricated molybdenum sulphide NPs were found to be much more efficacious at SOG than any other organic photosensitizer.

4.3 Porous-framework, carbon-based and hybrid nanoparticles

Distinct and tuneable optical as well as physicochemical properties have made carbon nanomaterials (NMs) an emerging potent class of materials for biomedical applications. Enhanced photostability, effective biocompatibility, chemical resistance, and tailorable fluorescence over a wide range of the visible to NIR-II spectrum make these NMs ideal candidates for *in vivo* molecular level imaging. Additionally, in accordance with recent findings it has been observed that Buckminsterfullerenes[91] and GQDs can be efficiently deployed as NPs for PDT which in turn could sensitize the generation of ROS.

Safar and his team of researchers came up with hybrid systems consisting of porphyrins and chirally enriched single walled carbon nanotubes (6,5-SWCNT). These systems proved to be ideal candidates for PDT.[92] The reported system was found to be much more efficient in terms of SOG when compared to neat, isolated porphyrins or E-SWCNT. This augmented performance stemmed from energy transfer from E-SWCNT to porphyrin which was finally transferred to O_2 molecules. Gao *et al.* prepared carbon nanodots which were passivated by using cetyltrimethylammonium ammonium bromide (CTAB-CDs). The optical properties of the nanodots were excellent and they were prepared by hydrothermally treating fullerene.[93] The CDs were found to significantly enhance and amplify the luminol–H_2O_2 chemiluminescence based signals. The CTAB-CDs could catalytically decompose hydrogen peroxide into $OH^{\bullet}$ and $O_2^{\bullet-}$. Subsequently, they recombined forming an avalanche of singlet oxygen on the surface of the fabricated CTAB-CDs.

Similarly, Knoblauch and his team reported the synthesis of bromine functionalized CDs.[94] These CDs were simple and inexpensive byproducts of hydrogen combustion. Metal-enhanced or amplified photosensitization of singlet oxygen species were reported with the usage of these brominated dots.

Blacha-Grzechnik *et al.* tailored a dyad structure *via* adopting electrochemical polymerization, thus forming layers of covalently conjugated photoactive poly(terthiophene) and fullerene.[95] SOG *via* the synthesized moieties was tested in the presence of a certain singlet oxygen quencher (2,3,4,5-tetraphenylcyclopentadienone) *via* a process known as α-terpinene oxidation.

Apart from fullerenes, graphene quantum dots have also gained immense momentum for PDT. GQDs have the innate ability to induce a synergistic effect of apoptosis as well as autophagy which in turn could effectively kill cancer cells.[96] GQDs generate oxidative stress and are highly efficient at SOG, thus causing the death of human glioma cell lines.

Kuo and his group fabricated TPE based GQDs with the help of a shearing reaction (ultrasonic). Such GQDs under TPE excitation for a mere 15 s produce huge amounts of singlet oxygen as well as O_2 molecules, thus eliminating both Gram positive and Gram negative bacteria.[97]

Chemically reduced GOQDs (rGOQDs) were also found to enhance and augment the ROS generation capacity yielding high amounts of $^1O_2$, O^{2-}, and H_2O_2 under irradiation of white light.[98] These rGOQDs possessed a greater number of electron–hole pairs owing to a low band gap and valence band compared to GOQDs. This resulted in a significant enhancement of ROS generation and higher efficacy for PDT.

Wang and his team functionalized and modified GQDs with adenine[99] and Xing's group covalently conjugated a rhodamine derivative (TRITC) along with UCNP-GQDs.[100] Both the modified GQDs were found to exhibit efficient *in vivo* PDT by SOG.

In the recent past researchers reported the usage of graphitic carbon nitride (g-C_3N_4) nanosheets for SOG in cancer PDT. Such nanoparticles showed significantly higher ROS generation when irradiated with LED and induced the death of HeLa cells.[101] Just like the nanosheets, HA modified graphitic hollow C_3N_4 nanospheres showed immense potential for stimuli-responsive chemotherapy as well as cancer PDT.[102] From this perspective Feng and his group conjugated UCNPs with g-C_3N_4 for the conversion of NIR into UV/Vis light that would match well with the absorption of g-C_3N_4 alone.[103] This could kill HeLa cells *via* an *in vitro* strategy.

Besides the techniques exemplified above, reticular chemistry has emerged as a promising area to develop nanomaterials for PDT. Porous and crystalline frameworks including covalent organic frameworks (COFs) and metal–organic frameworks (MOFs) represent a class of nanoagents that have proved to be extremely beneficial in the recent times.[104] Enhanced biocompatibility, tailorable porosity, design and structural flexibility, all add up to make these framework structures promising materials for PDT.[105] A Hf–porphyrin based nanoscale MOF was reported by Lin and his group. The MOF was composed of structurally regular moieties of Hf–oxo clusters and 5,15-di(*p*-benzoato)porphyrin bridging ligands.[106] The thin and uniform geometry of the material helped SOG through which cytotoxic effects were generated for the cancer cells. Similar MOFs were prepared by the same group, wherein

the ligand H_2DBP was reduced to 5,15-di(*p*-benzoato) chlorine.[107]

Lang and his team reported the fabrication of hexagonal PCN-222 in 2017. The MOF prepared could significantly induce apoptosis of tumor cells[108] *via* ROS generation upon visible light irradiation.

At the same time, a nanoscale MOF was reported by Tang *et al.* The nano-MOF was composed of zinc-metalated 5,10,15,20-tetrakis(4 methoxycarbonylphenyl) porphyrin and Cu^{2+}. The MOF termed NP-1 could act as a controlled PS for SOG *via* triggering of H_2S.[109] Motivated by this, numerous research groups around the globe have made significant contributions towards designing nanoscale MOFs for cancer PDT.[110–118]

In tandem with MOFs, nanoscale COFs also play a major role in cancer PDT. Although the research in this direction is still in its infancy, several groups have made notable progress in this area. In general porphyrin and its derivatives are usually utilized for SOG and they have been extensively reported for PDT. However, their poor solubility and agglomeration effects hinder their ready usability. To remedy such issues, COFs can be designed using a porphyrin derivative as the starting material.

Xie and his team fabricated a nanoscale composite (MOF@POP) termed UNM. It was made by the controlled growth of an imine-linked COF on the surface of an amine-functionalized MOF.[119] The system was found to be highly efficient in terms of SOG and thus was deployed for PDT. Deng *et al.* made use of species which were intrinsically incapable of SOG for the construction of a photosensitive COF (4,4′,4″-(1,4-phenylene)-bis([2,2′:6′,2″-terpyridine]-5,5″-dicarbaldehyde)). The ROS generation efficiency of the designed COF was found to be high owing to its band gap of 1.96 eV which linearly overlapped with the band gap of superoxide radicals.[120] Similarly, Zhang *et al.* synthesized an imine-based COF termed $COF_{TTA-DHTA}$ which had exceptional PDT efficacy *via* remodelling the extracellular matrix.[121]

4.4 Polymer-based nanoparticles

Contemporary research pertaining to PDT has gained a huge impetus in deploying biocompatible and biodegradable NPs based on polymeric materials.[122] Such polymeric species have the ability to selectively target specific organs and hence suitably control the release of photosensitizers. Emulsion as well as interfacial polymerizations have been mainly reported for the preparation of polymer-based nanoparticles. These nanoparticles can be nanocapsules or nanospheres, solely depending on the synthesis pathway adopted. Phthalocyanines are one of the most important and reported materials for PDT. However, one of the major bottlenecks associated with them is their inherent affinity towards aggregation which significantly reduces the SOG efficacy. As a remedy, several modifications have been carried out.

In 1991, tetrasulfonated zinc phthalocyanine ($ZnPcS_4$) and aluminium naphthalocyanine were synthesized and entrapped in nanocapsules made of poly(isobutylcyanoacrylate) or poly (ethylbutylcyanoacrylate).[123] Interfacial polymerization was employed to carry out the fabrication. The nanomaterial recorded near 100% efficiency for PS encapsulation. A novel "salt-out" method was employed for formulating a second-generation PS, *i.e.*, hexadecafluoro zinc phthalocyanine ($ZnPcF_{16}$) and subsequently encapsulating them in PEG-coated-PLA NPs.[124] With very low percentages of loading, high efficiency for PDT was observed for the material. Moreno and his team used polyacrylamide (PAA) and amine functionalized PAA as a matrix and loaded it with disulfonated 4,7-diphenyl-1,10-phenanthroline ruthenium [$Ru(dpp(SO_3)_2)_3$]. Such particles were able to exhibit high efficiency in SOG.[125] In a slightly different work, PS-loaded NPs were synthesized using a precursor which contained the PS unit as a copolymer. The copolymer, *i.e.* poly(phthalocyanine-*co*-sebacic anhydride) (Pc-SA), was formulated using the monomeric units of sebacic anhydride and Zn(II) phthalocyanine.[126] Here, with the PS loading being comparatively higher, quenching and entrapment of produced SOG is avoided, just leading to high SOG and hence greater usability in cancer PDT.

5. Utilizing conjugated polymers, copolymers, and nanocomposites, with a focus on enhancing singlet oxygen generation through dye-based and near-infrared (NIR) conjugated nanopolymers

Researchers are actively investigating novel approaches to photodynamic therapy (PDT), including the use of nanocomposites, copolymers, and conjugated polymers to increase the production of singlet oxygen. The strategic combination of dye-based and near-infrared (NIR) conjugated nanopolymers is the main focus, to increase the production efficiency of singlet oxygen.[127] This strategy, which demonstrates the development of PDT methodologies through the design and use of cutting-edge polymeric materials, is a sophisticated and focused approach. The synergistic combination of these elements shows a promising path toward the creation of more specialized and effective treatments for a range of illnesses, especially when it comes to the treatment of cancer.

One important family of organic molecules is conjugated polymers, which comprise considerable conjugated backbones and useful side chains.[128,129] Delocalized electrons migrate along the conjugated framework of conjugated polymers, allowing the energy collected by the backbone to be converted into optical signals *via* electronic transitions. This results in high fluorescence quantum yields and remarkable light-harvesting properties.

Developing dual-modal therapeutic systems for chemotherapy and PDT, the majority of conjugated polymers currently utilized as PSs are physically combined with medications. Yet, unreliable drug leakage could endanger healthy

tissues more severely and reduce the effectiveness of the combined anticancer effects.[130] In addition to improving the effectiveness of ROS generation, CPs can play beneficial roles in disease therapy. For example, a large number of side chains are commonly linked to the CP backbones, which may facilitate drug dispersion and responsive drug release. Another illustration is the photothermal effect, whereby CPs frequently function as good photothermal agents due to their large molar extinction coefficients, provided that the near-infrared (NIR) absorption is regulated. For this reason, synergistic therapy in conjunction with photothermal therapy (PTT) or chemotherapy is another strategy to improve CP-based PDT.

Therefore, we discuss here the most recent studies of singlet oxygen generation for PDT employing conjugated polymers, copolymers, nanocomposites, or nano-conjugated polymers. Numerous studies reported in the literature are provided here.

Battah *et al.*[131] reported the synthesis of hydroxypyridinone and 5-aminolaevulinic acid conjugates while Wang *et al.*[132] synthesized hemoglobin (Hb) conjugates with polymeric micelles formed by triblock copolymers of poly(ethylene glycol)-*block*-poly(acrylic acid)-*block*-polystyrene (PEG-*b*-PAA-*b*-PS) through chemical conjugation. *In vitro*, HeLa cells were more susceptible to photocytotoxicity and increased the generation of $^1O_2$ by the Hb-coupled photosensitizer carrier (Fig. 17).

Yesilgul *et al.*[10] synthesized an erythrosine–luminol conjugate for singlet oxygen generation with chemical excitation. Spada *et al.*[133] created conjugated poly(9,9-dioctylfluorene-alt-benzothiadiazole) (F8BT) doped with platinum octaethyl porphyrin (PtOEP) which was able to efficiently generate singlet oxygen. According to Cheng *et al.*,[134] mesoporous silica nanoparticles (MSNs) were functionalized with Pd–porphyrins to produce MSN–PdTPP, which might be used as phosphorescence probes for oxygen detection and tomography. Poly [(9,9-dioctylfluorenyl-2,7-diyl)-*alt-co*-(1,4-benzo-{2,1′,3}-thiadiazole)] was developed by Chang *et al.*[135] Porphyrin was integrated into the π-conjugated backbone to enable photodynamic treatment that was sensitive to polymer dots.

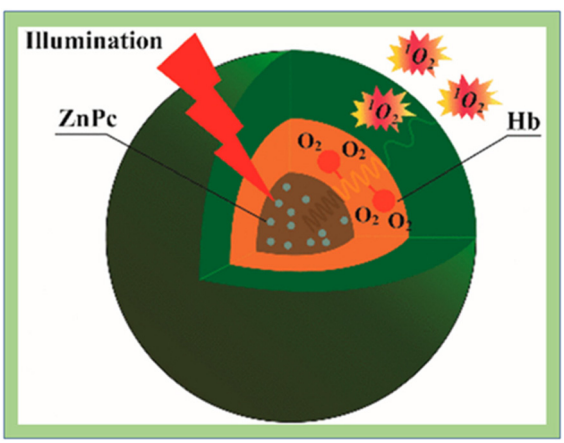

Fig. 17 Singlet oxygen generation in ZnPC loaded HbMs. Reproduced with permission.[132] Copyright 2015, American Chemical Society.

Islam *et al.* synthesized a nano-formulation of 5-aminolevulinic acid (5-ALA) for tumour-targeted photodynamic treatment. P-ALA was obtained by coupling 5-ALA with the biocompatible polymer *N*-(2-droxypropyl)methacrylamide (HPMA) *via* the hydrazone link. P-ALA functions as a nanoscale molecule in an aqueous solution due to its average size of 5.5 nm. P-ALA was discovered to be non-cytotoxic up to 0.1 mg ml^{-1}; but, at an IC50 of 20–30 g mL^{-1}, it was observed to cause a significant degree of cell death when exposed to light. Most significantly, they found that 5-ALA, which profited from its nano-size by utilizing the enhanced permeability and retention (EPR) effect, was less likely to significantly accumulate in tumours than P-ALA. According to the authors, P-ALA exposure greatly enhanced *in vivo* anticancer activity without exhibiting any observable negative effects. As such, they hope to employ P-ALA as a nano-engineered photosensitizer for photodynamic treatment of cancer.[136]

A modest number of red-emitting TBT units doped with poly[9,9′-bis(2-(2-(2-bromoethoxy) ethoxy)ethyl)fluorene-2,7-ylene vinylene] was used by Huang *et al.* to develop novel zwitterionic red-emitting water-soluble conjugated polymers P1′ and P1″. Through the use of TPE FRET, red emission from the poly(fluorene-2,7-ylene vinylene) segments (donor) to the TBT units (acceptor) was detected for both P1′ and P1″. The authors reported that fluorescence resonance energy transfer (FRET) was used by P1′ and P1″ to accomplish TPE red emission. They discovered that P1″ had a significantly greater $^1O_2$ quantum yield (61%) than P1′, which was just 39%. They proposed that zwitterionic P1″ had been verified to exhibit promise as a superior TPE red-emitting photosensitizer for PDT guided by two-photon imaging.[137]

Shen and colleagues synthesised tetraphenylporphyrin (TPP) doped poly[9,9-dibromohexylfluorene-2,7-ylenethylene-*alt*-1,4-(2,5-dimethoxy)phenylene] nanoparticles (PFEMO). In living cancer cells, conjugated polymer nanoparticles doped with photosensitizers exhibit improved singlet oxygen generation and potent photodynamic treatment efficacy. The two-photon light-harvesting complex and the host material were made from the conjugated polymer PFEMO. Under one- and two-photon stimulation, enhanced singlet oxygen generation was reported[138] (Fig. 18).

Ren *et al.* carefully planned and developed a new fully organic UIM of THPP-4PMMA-*b*-4P(PEGMA-*co*-APMA) @NIR-800 having a dual PTT/PDT purpose. MMA and PEGMA/BAPMA were sequentially polymerized using the photocontrolled BIT-RDRP technique after four-armed porphyrin-based initiators were first created. Due to the ability of ketocyanine to undergo photothermal conversion and the release of singlet oxygen from the porphyrin segment, the produced star-shaped block copolymer could produce UIMs with a diameter of approximately 13.1 nm in water at a concentration lower than CAC. Through PDT and/or PTT of the UIMs, excellent biocompatibility, minimal cytotoxicity, and great tumour therapy were revealed. More effective behavior was suggested through utilizing the PDT/PTT synergistic effect.[139]

A three-dimensional (3D) organic–inorganic photosensitizer made of a stiff POSS cage with dodecyl alkyl chains on its glob-

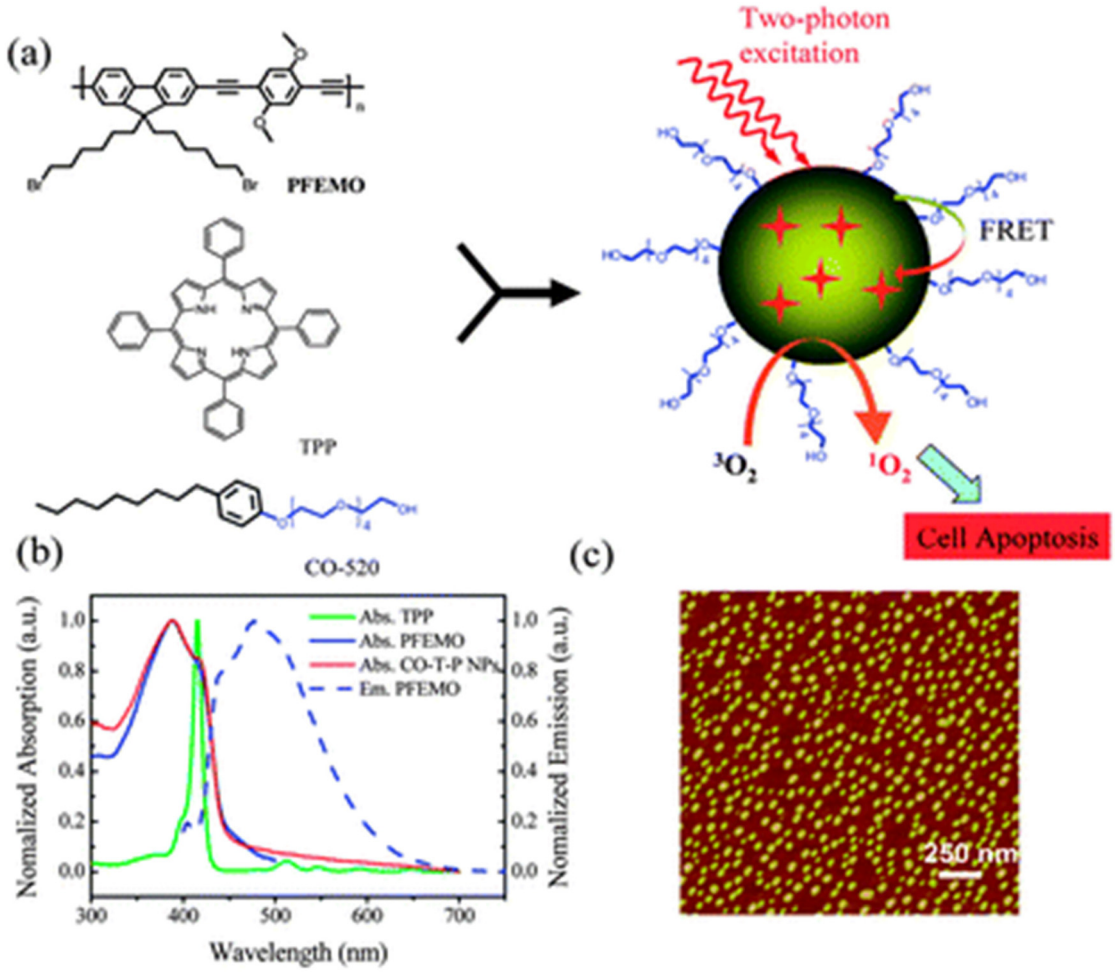

Fig. 18 (a) Diagram showing the process of conjugated polymer nanoparticle formation for two-photon photodynamic therapy; (b) normalized absorption spectra of TPP, PFEMO and CO-T-P NPs (solid lines), and emission spectra of PFEMO (dashed line); (c) AFM imaging of CO-T-P NPs on a mica substation. Reproduced with permission.[138] Copyright 2011, Royal Society of Chemistry.

ular exterior and a porphyrin core was claimed to have been synthesized by Bao *et al.* Then, using a co-precipitation technique, PorPOSSC12 was encapsulated in the polymer matrix using two different types of semiconducting polymers with various fluorescence colours. In addition to efficiently preventing the photosensitizer from aggregating, the hydrophobic semiconducting polymer backbones can also be partially separated by the 3D nanostructure of POSS and the covalently attached to dodecyl alkyl, which helps to lessen fluorescence quenching caused by aggregation. The scientists speculate that as a result, the PorPOSSC12-doped SPNs may function effectively as photodynamic nanoagents for the treatment of cancer and as fluorescent probes for bioimaging[140] (Fig. 19).

Tetraphenylethylene-1-phenyvinyl-pyridine-phenylboronic acid (TPEPy-BA) and tetraphenylethylene-1-phenyvinyl-pyridine-phenylboronic acid pinacol ester (TPEPy-BE), two novel aggregation-induced emission-based photosensitizers, were developed and synthesized by Sauraj and his colleagues. In order to increase the photosensitizers' water stability and cellular take up, they were also encapsulated within a copolymer (DSPE-PEG). The synthesized photosensitizer nanoparticles established a high intracellular reactive oxygen species generation efficacy. They observed that, when exposed to white light, tetraphenylethylene-1-phenyvinyl-pyridine-phenylboronic acid pinacol ester nanoparticles significantly outperformed tetraphenylethylene-1-phenyvinyl-pyridine-phenylboronic acid nanoparticles in terms of the photodynamic ablation of MCF-7 cells.[141]

Wang *et al.* rationally developed and produced mono- and tetra-nuclear Ir(III) complex–porphyrin conjugates, with **[TPP-4Ir]$^{4+}$** showing blatant aggregation-induced emission (AIE) properties. PSs made of Ir(III) complex–porphyrin conjugates were successfully achieved as nanoparticles (NPs). Moreover, **[TPP-4Ir]$^{4+}$** NPs display strong cytotoxicity against cancer cells, decent biocompatibility, high $^1O_2$ generation capacity, low half-maximal inhibitory concentration (IC_{50}) (0.47 106 M), and improved cellular take up when exposed to white light. The claim that transition metal complex PSs have exciting potential applications in medicine is expanded by that work[142] (Fig. 20).

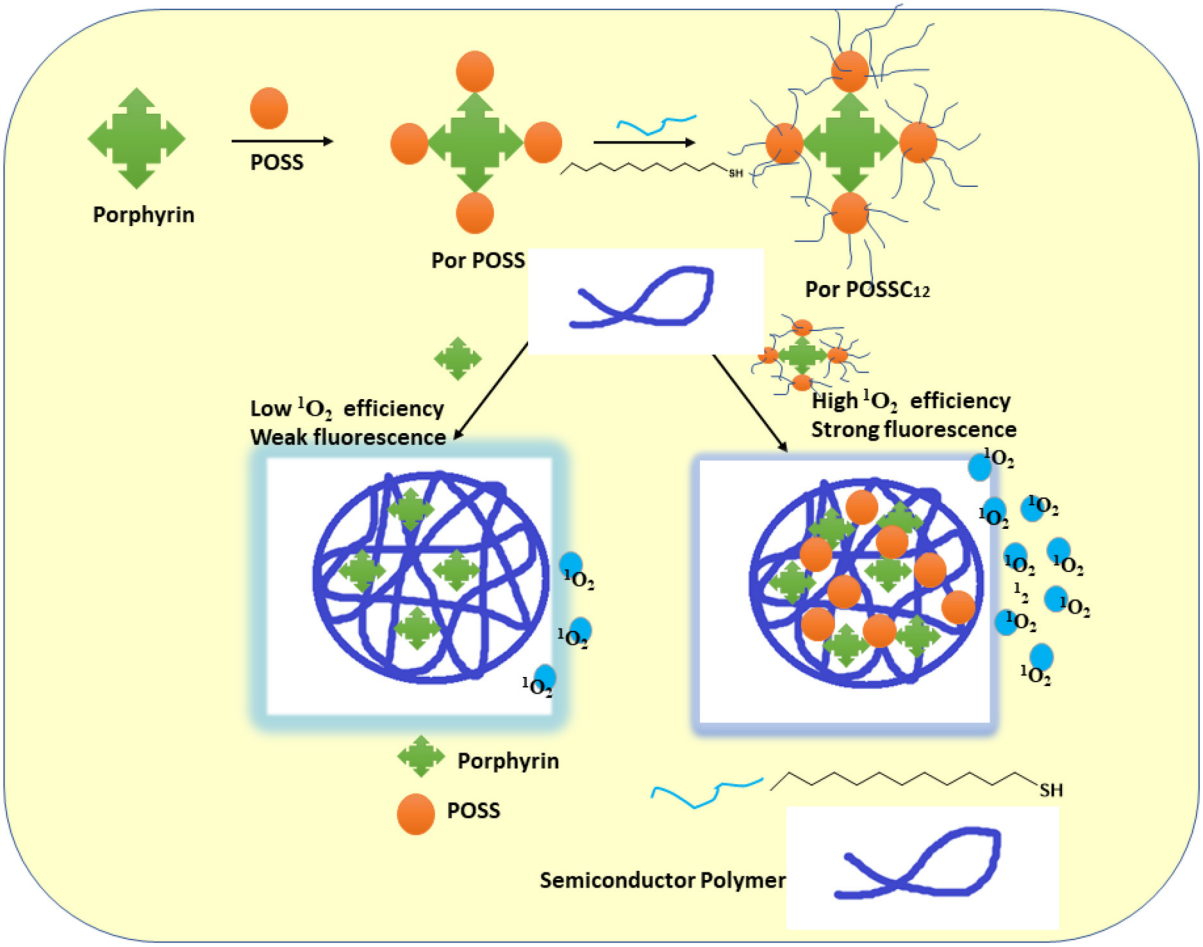

Fig. 19 A schematic representation of the PorPOSSC12-doped SPN architecture, together with the way that fluorescence imaging is improved and its suitability for application in PDT is increased (*this image was taken from* ref. 140).

Chen and coworkers developed aza-boron-dipyrromethene (Aza-BODIPY) with 2,6-diiodo-dipyrromethene (2,6-Diiodo-BODIPY) to create a near-infrared (NIR) chemical agent. Aza/I-BDP nanoparticles (NPs) were formed by enclosing them in DSPE-mPEG5000, an amphiphilic biocompatible copolymer. They noticed that the produced NPs showed an amazing photostability, a high quantum yield ($\Phi\Delta$ = 59%) of $^1O_2$ generation, and good photothermal conversion efficiency[143] (Fig. 21).

Tetratroxaminobenzene porphyrin-loaded biodegradable silk nanospheres (NSs) were synthesized by Cheng *et al.* using the emulsion–solvent–evaporation method. In order to achieve a greater photoconversion efficiency and a quicker synthesis of active oxygen, TAPP was chosen as the fundamental unit of the photosensitizer and then allowed to self-assemble into biodegradable silk. Furthermore, these self-assembled structures display increased singlet oxygen-generating capability and PDT performances, according to the authors[144] (Fig. 22).

Vinita *et al.* designed a surface charge augmented nanoconjugate system that decreased Pi3K/AKT indicating and decreased cell survival. To create the nanoconjugate system, the S–H group in triphenylphosphonium (TPP) was conjugated with both cationic and anionic AuNTs. The surface charge increased AuNTs combined with TPP exhibit cytotoxicity under 5-ALA-based PDT. Due to the generation of ROS species and the deregulation of mitochondria, DNA damage causes the induction of apoptosis. Together, 5-ALA and PDT with gold nanoconjugates help breast cancer cells undergo apoptosis. The created gold nanoconjugate system, according to the author, is an effective anti-cancer medication that targets mitochondria and causes cellular apoptosis in breast cancer.[145]

A unique triarylamine (TPA)-modified hemithioindigo (HTI)-based aggregation-induced emission (AIE) photosensitizer, 6Br-HTI-TPA-OMe, was successfully developed by Wang *et al.*, who found that reversible control over $^1O_2$ generation was possible due to the covalent link between the triarylamine AIE photosensitizing moiety and the HTI switch unit. The nanoparticles (NPs) synthesized from amphiphilic phospholipids also displayed photochromic activity in water. After receiving 520 nm light from an LED, the *Z*-NPs started to produce $^1O_2$, but when switching to the *E*-NPs, viable energy transfer prevented $^1O_2$ production. The authors suggested that reversible *Z*/*E* isomerization could photocontrol $^1O_2$ production. The ability of 6Br-HTI-TPA-OMe to function as a photoswitchable

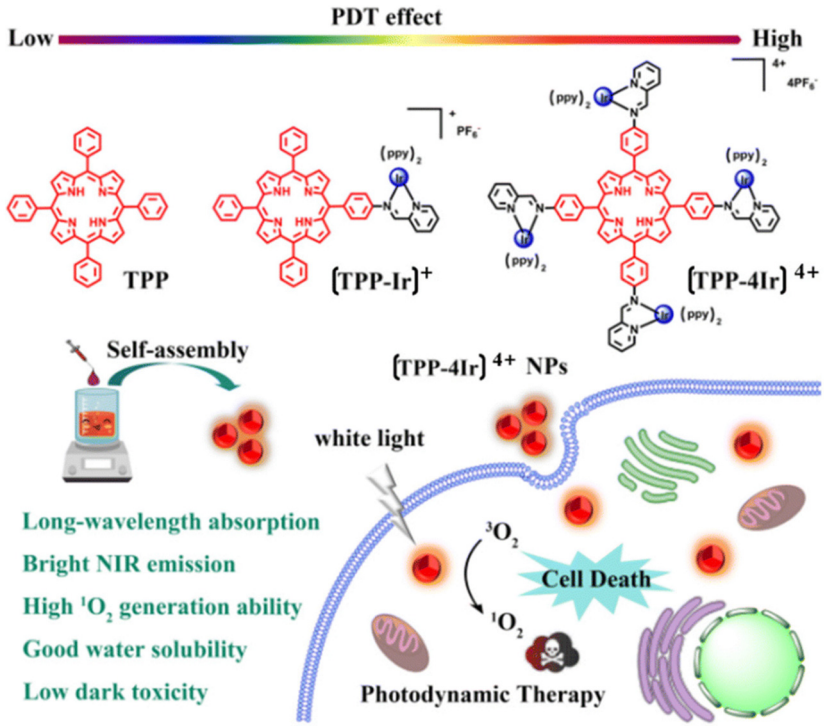

Fig. 20 Chemical structures of **TPP**, **[TPP-Ir]$^{+}$** and **[TPP-4Ir]$^{4+}$** and design principle of using **[TPP-4Ir]$^{4+}$** as PS for PDT.[142]

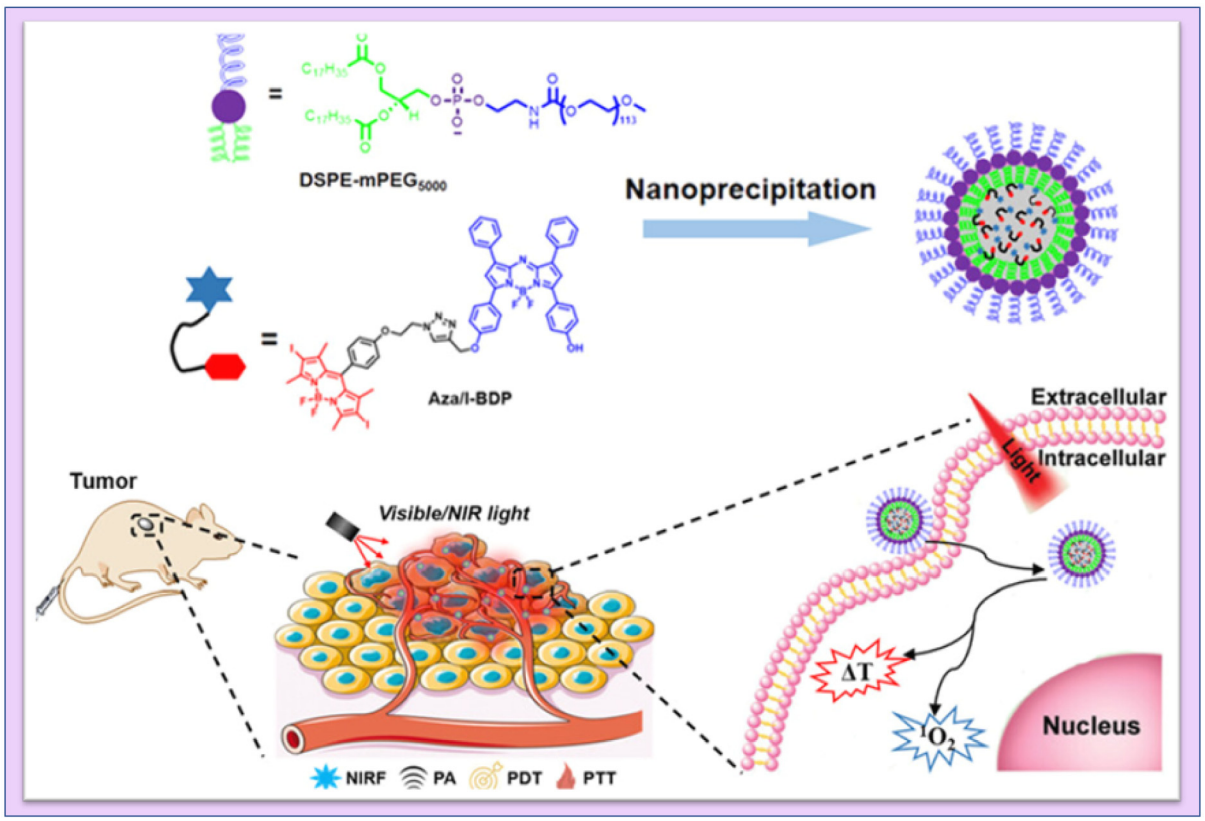

Fig. 21 Schematic illustration of the mechanism of fluorescence/PA imaging-guided tumor PDT/PTT by Aza/I-BDP NPs. Reproduced with permission.[143] Copyright 2023, American Chemical Society.

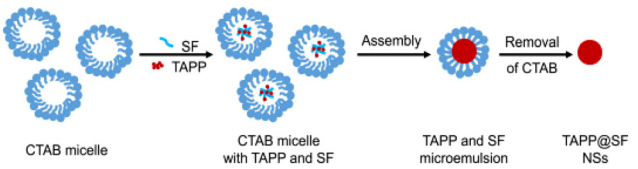

Fig. 22 Schematic representation of preparing TAPP NSs. Reproduced with permission.[144] Copyright 2023, Elsevier.

AIE photosensitizer was confirmed by an *in vitro* anti-tumor experiment[146] (Fig. 23).

Zhao *et al.* synthesized a conjugated oligomer called UF-TTOEH-2Cl, which had a photoactive acceptor (A)–donor (D)–acceptor (A) structure. They used UF-TTOEH-2Cl to create a folic acid-functionalized amphiphilic block copolymer named FA-PEG-PBLA10 through a nanoprecipitation technique. This material exhibited a high photothermal conversion efficiency of 42% and a singlet oxygen ($^1O_2$) quantum yield ($\Phi\Delta$) of 17.2% when exposed to an 880 nm laser. Furthermore, they demonstrated the effectiveness of photodynamic therapy (PDT) and photothermal therapy (PTT) synergistic treatment for malignancies using UF-TTOEH-2Cl-based nanoparticles in an *in vitro* setting. They tested this approach on HeLa and SiHa cells, which are commonly used as models in cancer research. This research suggests that these nanoparticles (UTNPs) have potential applications in combined PDT and PTT for cancer treatment[147] (Fig. 24).

Diaxial ethyl vanillin, a bioactive molecule substituted for silicon phthalocyanine, was designed by Karanlak *et al.* Photophysicochemical and sono-photochemical tests were carried out. In contrast to the photodynamic application, the sono-photodynamic application, which combines the syner-

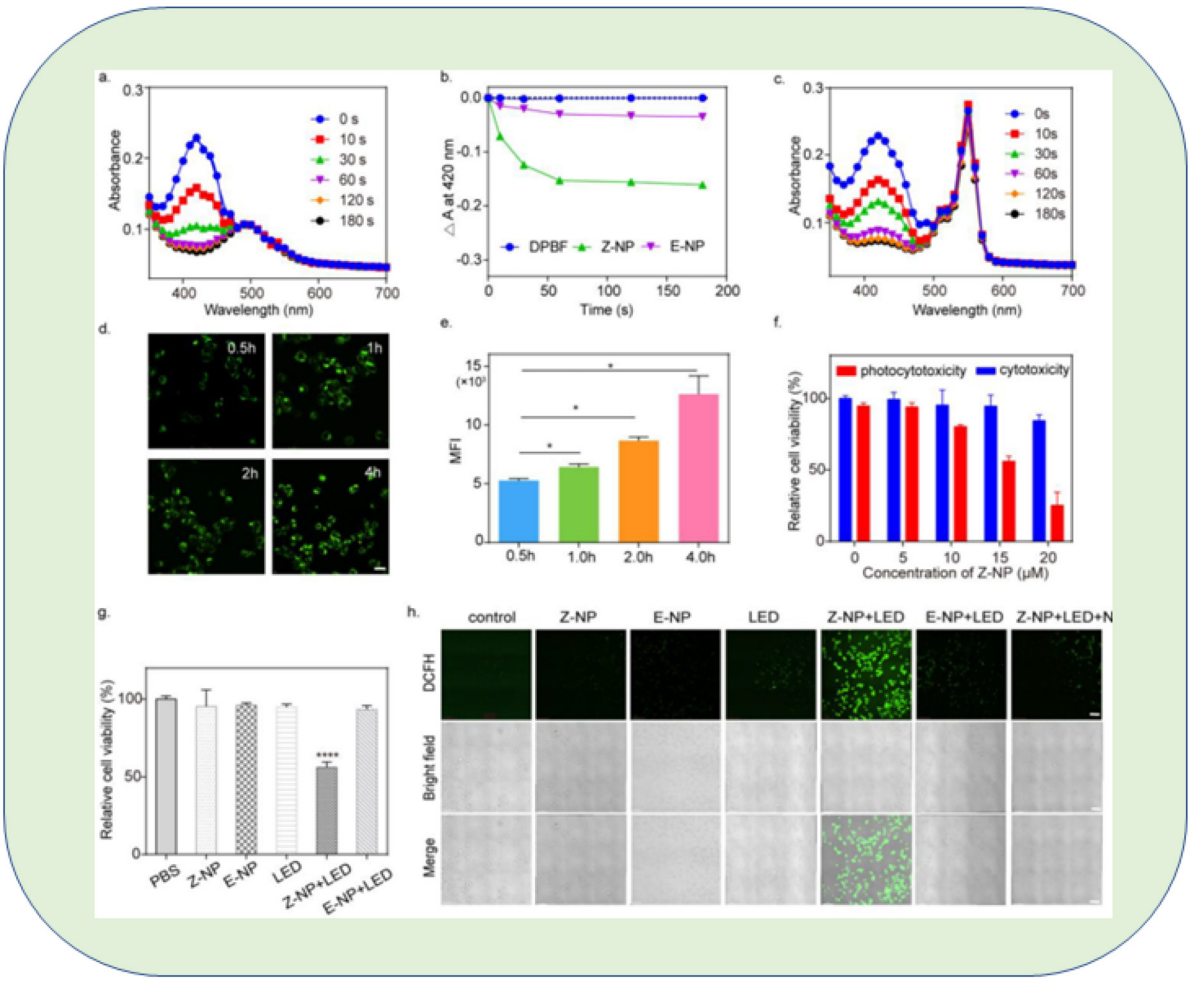

Fig. 23 *In vitro* evaluation of 6Br-HTI-TPA-OMe NPs for reversible control of $^1O_2$ generation. (a) Absorption spectra of DPBF (30 μM) with *Z*-NP (*Z* isomer concentration: 10 μM) in water at different irradiation times. (b) Photodegradation rate of DPBF with or without different nano-photosensitizers. (c) Absorption spectra of DPBF (30 μM) with RB (10 μM) in water at different irradiation times. Real-time take up images (d) and flow cytometry MFI value (e) of *Z*-NPs (15 μM) in 4T1 cells at different time points (0.5 h, 1 h, 2 h, 4 h). (f) MTS assay of *Z*-NPs at various concentrations co-cultured with 4T1 cells with or without LED irradiation (LED: 520 nm, 40 mW cm^{-2}, 5 min). (g) MTS assay of 4T1 cells incubated with different treatments. (h) Confocal images of 4T1 cells stained with DCFH-DA after different treatments. The treatments included PBS, *Z*-NPs, *E*-NPs, LED, *Z*-NP + LED, *E*-NP + LED, *Z*-NP + LED + NaN3 (*Z* isomer concentration: 15 μM, NaN_3 concentration: 20 mM, 520 nm, 40 mW cm^{-2}, 5 min, scale bar: 100 μm). Significant differences between the groups are labelled for * $p < 0.05$, and **** for $p < 0.0001$.[146]

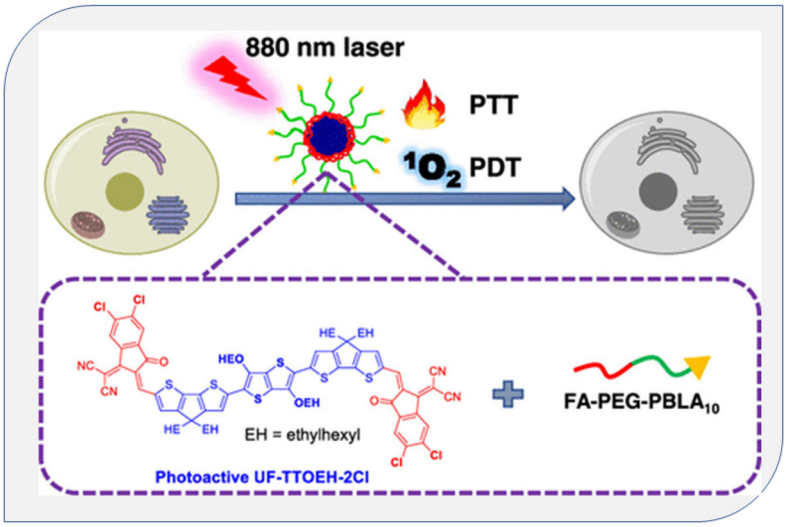

Fig. 24 Diagram of singlet oxygen generation from conjugated polymers in PDT. Reproduced with permission.[147] Copyright 2023, American Chemical Society.

getic action of light and ultrasound together as a stimulation approach, increased singlet oxygen production through photochemical measures from 0.50 to 0.81. It is therefore appropriate as an excellent sensitizing agent in both PDT and SPDT given the molecule's photostability and high singlet oxygen production ability for both techniques.[148]

In a similar way, pyrazoline-fused axial silicon phthalocyanine (HY-SiPc), peripheral zinc phthalocyanine (HY-ZnPcp), and non-peripheral zinc phthalocyanine (HY-ZnPcnp) were all designed and synthesized by Yalazan and colleagues. They looked at and researched the roles that silicon phthalocyanine compounds with methoxylated pyrazoline groups played in both photophysical and photochemical processes. The authors suggested that, the HY-ZnPcp molecule, $\Phi\Delta$ 0.73%, which produced the most singlet oxygen among the three produced phthalocyanines (HY-ZnPcp, HY-ZnPcnp, and HY-SiPc), could be regarded as a photosensitizer candidate for PDT.[149]

Liu *et al.* used an innovative reversible addition–fragmentation chain transfer (RAFT) polymerization method to create a thermosensitive star-shaped double hydrophilic polymer called THPP-(PNIPAM-*b*-PMAGA)$_4$. This polymer consists of poly(*N*-isopropylacrylamide) (PNIPAM) and poly(methylacrylamide glucose) (PMAGA) block copolymers. The values of $\Phi\Delta$ for different molecular weights of THPP-(PNIPAM-*b*-PMAGA)$_4$ in dimethylformamide (DMF) were found to be 0.41 and 0.37. In summary, THPP-(PNIPAM-*b*-PMAGA)$_4$ holds promise as a potential photodynamic therapy (PDT) reagent. It can be used as a photosensitizer for PDT. However, it is worth noting that this compound exhibits significant toxicity when exposed to light in the presence of HeLa cells. This research paper presents a novel approach that combines chemotherapy and PDT for tumor targeting, aiming to advance cancer treatment strategies.[150]

In order to enhance phototherapy and enable real-time $^1O_2$ self-detection and O_2 self-supply, Yang *et al.* developed a nanosensor known as PAPD, which blended dual-channel ratiometric sensing with oxygen-augmenting approaches. An anthracene-based $^1O_2$ sensitive fluorophore (DPA) was encapsulated in porphyrin metal–organic frameworks (PCN-224) and gold nanoparticles (AuNPs) were used as nano-enzymes to create the PAPD nano-sensor. The Au–S link was used to cover polyethylene glycol thiol (PEG-SH). PCN-224 is utilized as a photosensitizer and $^1O_2$ reference fluorescence (FL) agent. After PCN-224-induced $^1O_2$ is synthesized, the dual-channel ratio-metric FL signal of PAPD generates a dynamic, sensitive, and accurate $^1O_2$ visualization and offers real-time therapeutic data related to the therapeutic procedure. Furthermore, the catalase-like activity of PAPD produces O_2 *in situ* by intracellular H_2O_2 oxidation and increases the $^1O_2$ yield, which increases the effectiveness of destroying tumour cells. They claimed that the rationally designed nanosensor PAPD offered a paradigm for clinically precise hypoxic tumour treatment and real-time therapeutic evaluation[151] (Fig. 25).

Tan *et al.* developed a synthesis method to create a conjugate called HES-SeSe-DOX with a high loading of the anticancer drug DOX. These conjugates, when accumulated in the form of nanoparticles (NPs) along with Ce6 (a photosensitizer), can respond to stimuli that affect diselenide bonds. When these bonds are disrupted, it leads to the cascade release of DOX and Ce6. Simultaneously, the seleninic acid formed from the broken diselenide bonds can work in conjunction with DOX and Ce6 to enhance the inhibition of tumor cell growth. These HES-SeSe-DOX/Ce6 NPs, which have received limited attention from researchers thus far, hold the potential to be a novel class of nanomedicine. To assess whether these NPs can enhance chemo-photodynamic anticancer therapy, comprehensive investigations of their *in vitro* and *in vivo* performances have been conducted. This research aims to explore their effectiveness as a promising approach for cancer treatment.[152]

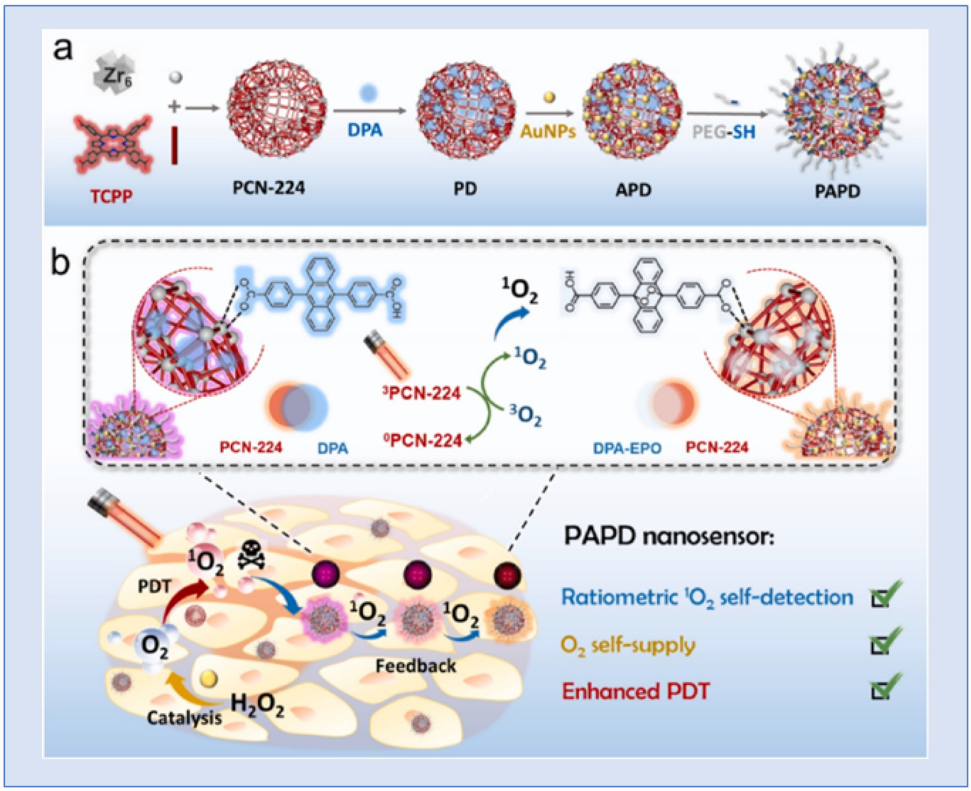

Fig. 25 Representation of (a) PAPD preparation and (b) multifunctional integration of ratiometric $^1O_2$ self-detection, O_2 self-supply and enhanced PDT. Reproduced with permission.[151] Copyright 2023, Elsevier.

The evolution of conjugated polymers for photodynamic therapy (PDT) constitutes a dynamic trajectory in cancer treatment research. Initially recognized for their advantageous properties, such as high fluorescence efficiency, remarkable photostability, and potent light absorption, conjugated polymers have emerged as promising candidates for PDT applications. Researchers have systematically delved into the development of these polymers, employing sophisticated chemical synthesis techniques and flexible polymer architectures to engineer variants with heightened singlet-oxygen generation capabilities, a crucial factor for the success of PDT. Beyond isolated examples, the overarching trend involves the strategic design of conjugated polymers tailored for optimal performance in PDT. The incorporation of photosensitizers into conjugated polymer nanoparticles is particularly noteworthy, as it enhances singlet-oxygen formation through efficient energy transfer. Moreover, the integration of nanotechnology has opened new avenues, offering innovative solutions to enhance photosensitizer performance and address challenges in cancer PDT. In summary, the development of conjugated polymers for PDT reflects a comprehensive and systematic approach, capitalizing on their inherent qualities and utilizing advanced synthesis methods to propel the field towards more effective cancer treatment modalities.

Dyes have been widely used in fluorophore moieties because of their outstanding photophysical properties and because of their ability to demonstrate good singlet oxygen production that is successfully applicable in PDT. Researchers have been exploring various types of dyes incorporated into conjugated polymers for singlet oxygen generation in PDT.

Singh *et al.* reported on singlet oxygen generation and the anticancer activity of polymerizing 1,4-benzoquinone (BQ), Amido Black 10B (AB-10B), and Alizarin Red (AR) with *o*- and *p*-phenylenediamines using ultrasound assistance for the first time.[153] According to Singh and colleagues, lawsone (LW) was integrated into conjugated polymers of pyrrole, thiophene, *p*-phenylenediamine, and 1-naphthylamine using an ultrasound-assisted technique. The $^1O_2$ generation investigation, according to the authors, was conducted using the DPBF test, which showed the highest quantum yield value of 0.11 for Ppy-LW. Additionally, they proposed that LW might be used in photodynamic therapy because it was an easy way to adjust fluorescence emission and singlet oxygen formation in conjugated polymers.[154] The same group also designed *ortho*-phenylenediamine with 1,4-benzoquinone, which enabled the efficient production of singlet oxygen ($^1O_2$). According to the researchers, $^1O_2$ generation investigations showed that the oligomer with the highest quantum yield value of 0.057 was composed of 70% benzoquinone. They proposed that their findings could be useful in the application of engineered oligomers as photosensitive probes for photodynamic treatment.[155] Singh *et al.* also reported novel azo benzene functionalized aniline, 1-naphthylamine, luminol and *o*-phenylenediamine prepared by using an ultrasound technique. The researchers

suggested that the synthesized polymers also showed high singlet oxygen generation characteristics.[156]

From 700 to 1100 nm, biological systems are transparent to NIR light. It is possible to manipulate light in this optical window while causing the least amount of harm to tissues and organs. A possible noninvasive cancer treatment method is photothermal therapy (PTT). By stabilizing the quinoid resonance structure, extending the large conjugated region, or employing D–A (donor–acceptor) exchanges in conjugated molecules, one is able to accomplish a low band gap in conjugated molecules, which satisfies the need for identifying the absorption in the biosafety optical window.[157] Many groups are exploring the use of conjugated polymers (CPs) for photothermal cancer treatment because many of these polymers have high near-infrared (NIR) absorbance, making them promising candidates for this purpose.[158]

In image-guided photodynamic cancer therapy, using a photosensitizer that operates in the far-red (FR) or near-infrared (NIR) range is highly desirable. Wu *et al.* achieved this by employing a one-pot Suzuki polymerization process to create a polymer known as PTPEAQ. This polymer contains anthraquinone (AQ) as an electron acceptor and tetraphenylethylene (TPE), a well-known aggregation-induced emission (AIE) active group, as an electron donor. They further developed PTPEAQ-NP-HER2 by encapsulating PTPEAQ within a block copolymer and modifying its surface with an anti-Her2 antibody. PTPEAQ-NP-HER2 exhibits impressive AIE-active emission in the FR/NIR range and can efficiently generate singlet oxygen when exposed to visible light. This unique property has been successfully harnessed for the photodynamic ablation of cancer cells. They specifically demonstrated its effectiveness using SKBR-3 cells, a type of breast cancer cell characterized by overexpression of the HER2 receptor on the cell membrane[159] (Fig. 26). Two cationic AIE active polymers, DCPN-1 and DCPN-2, were formed and synthesized by Cong *et al.* using the ring opening polymerization method. The majority of the visible light spectrum was covered by the intense emissions that DCPN-2 emits in the NIR region (>650 nm), and it efficiently produces reactive oxygen species (ROS) when exposed to light. Prominently, it was shown both *in vitro* and *in vivo* that DCPN-2 administration during light irradiation inhibited tumour growth.[160]

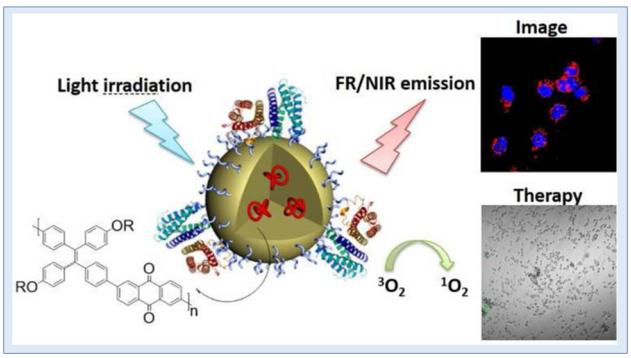

Fig. 26 NIR conjugated polymers showing singlet oxygen generation and PDT. Reproduced with permission.[159] Copyright 2016, American Chemical Society.

Recent studies have concentrated on dual-modal imaging-guided phototherapy employing near-infrared fluorescence (NIRF) and photoacoustic (PA) techniques. One of the main challenges is creating a theranostic tool that is easy to use and efficient at improving photodynamic therapy (PDT) and imaging-guided photothermal therapy (PTT). In the study by Tan *et al.*, Ag@PANI nanocomposites loaded with ICG as a theranostic agent for imaging-guided phototherapy are a promising way to advance cancer therapy, as their work suggests. These nanocomposites have the potential to be useful in solving cancer therapeutic issues due to their unique combination of features, which include excellent NIR absorption, improved photostability, efficient development of hyperthermia, and maintained ROS production. These results open up new possibilities for the theranostic treatment of cancer, where it can be used to fight tumours with more accuracy and efficacy.[161]

Sun and colleagues created and produced thiophene (TPA-TDPP), diketopyrrolopyrrole (DPP) core functionalized benzene (PDDP), and derivatives of benzene (TPA-PDDP). To prove the heavy atom effect, they ran electrochemistry experiments. TPA-TDPP's energy level dropped when triphenylamine (TPA) was added, and a 50% quantum yield increase in the synthesis of singlet oxygen ($^1O_2$) was observed. Additionally, they increased the power conversion efficiency (PCE) of TPA-TDPP to 38.7% by adding thiophene, triphenylamine, and long alkyl chains in the aggregated form. This was achieved by encouraging a twisting action and lowering intermolecular contact. TPA-TDPP nanoparticles' enhanced permeability and retention (EPR) effect allowed for the targeting of tumour regions, as demonstrated by *in vivo* fluorescence imaging. These nanoparticles showed remarkable photodynamic/photothermal synergy.[162]

Nave *et al.* created a novel, straightforward technique for creating NIR light-responsive nano-systems that were utilized in cancer chemo-photodynamic/photothermal treatment. They accomplished this by creating an amphiphilic conjugate of poly(2-ethyl-2-oxazoline)-IR780 that, when combined, might encase doxorubicin (DOX/PEtOx-IR NPs) and have photodynamic/photothermal characteristics. The size and surface charge of the DOX/PEtOx-IR NPs were advantageous for applications linked to cancer. When exposed to NIR light, the DOX/PEtOx-IR NPs boosted the release of DOX by 1.7 times while producing singlet oxygen and a lower thermic impact. DOX/PEtOx-IR NPs and NIR light were able to entirely eradicate breast cancer cells (viability 4%) in *in vitro* experiments; this is representative of the improved outcomes from the chemo-photodynamic/photothermal treatment presented by the nanomaterials.[163]

Chen and colleagues effectively synthesized an NIR coumarin-BODIPY photosensitizer BDP-C with iodine for photodynamic treatment using a Knoevenagel condensation process. The maximum wavelengths of BDP-C's emission and absorption were 732 nm and 808 nm, respectively. 2.13×10^5 cm^{-1} M1

was found to be the highest molar absorption coefficient. After being exposed to radiation, BDP-C showed an outstanding long-term cell imaging capability, strong photostability, and good biocompatibility. It also had a moderate singlet oxygen quantum yield. According to *in vitro* research, BDP-C can be selectively localized in lysosomes where it can effectively destroy cancer cells when exposed to radiation. Overall, they demonstrated an NIR organic PDT photosensitizer, and BDP-C could serve as a viable substitute for any PDT photosensitizer based on BODIPY used in medical settings in the future.[164]

Owing to the benefits of two-photon excited phototherapy, as demonstrated by Wu and his coworkers, immense research interest have developed in the scientific community in this direction. The lack of a high-performance photosensitizer with broad two-photon absorption cross-sections and specialized targeting capabilities renders phototherapy ineffective in the treatment of cancer. Here, a new photosensitizer, 6DBF2, derived from BODIPY was developed with two-photon photosensitization for *in vivo* two-photon stimulated photodynamic treatment. Following near-infrared laser activation, 6DBF2 exhibits strong two-photon absorption and effective $^1O_2$ production. The exceptional therapeutic effectiveness of 6DBF2 in two-photon stimulated photodynamic treatment was demonstrated by *in vivo* tumour ablation inside mouse models and *in vitro* cancer cell ablation following NIR two-photon irradiation. The authors reported a unique instance of lipid droplets that were targeted by photodynamic radiation allowing deep tumor cell imaging and treatment with near-infrared light irradiation.[165]

Wu and colleagues created novel organic photothermal nano-agents in the near-infrared (NIR) range by utilizing conjugated boron dipyrromethene (BODIPY) oligomers as a support. These nanomaterials showed outstanding photostability, tunable NIR absorptions, and a very effective conversion of NIR light to heat. Under NIR laser light, they may efficiently accumulate in tumour tissues and accomplish total tumour ablation. This strategy, known as "excited-state rotation, ground-state conjugation", offers a state-of-the-art framework for creating sophisticated theranostic compounds with near-infrared absorption for a range of therapeutic uses.[166]

Recent years have seen an increase in phototherapeutic techniques like photodynamic therapy (PDT) and photothermal treatment (PTT) that have attracted significant attention in biological and medicinal fields. The key to maximizing therapeutic effectiveness is to discover potential compounds with beneficial PDT and PTT interaction effects, particularly those brought on by single-wavelength NIR light. A low-bandgap fluorene-based donor–acceptor–donor (D–A–D) conjugated oligomer, synthesized in a green pathway showed a broad absorption in both the visible and NIR ranges, according to Peng *et al.* The authors demonstrated that the oligomer had a good photothermal capacity with a conversion efficiency of 37.7% after being exposed to an 808 nm laser, along with concurrent photodynamic behavior that led to the production of reactive oxygen species. Additionally, its green fluorescence, which was stimulated by 420 nm light, offers the chance for imaging-guided therapy.[167]

6. Outlook and future prospects

Photodynamic therapy (PDT) involves interactions between reactive $^1O_2$, light, and photosensitizers. Treatment responses vary significantly within and between lesions due to differences in vascular status and the microenvironment. Therefore, it appears to be challenging to accurately determine the required light dose and photosensitizer dose. Over the past 10 years, there have been notable and significant advancements in research towards the creation of nanomaterials that elicit the production of singlet oxygen ($^1O_2$) with a high quantum yield. Due to their extensive usefulness in photodynamic therapy (PDT), these compounds have garnered significant attention within the scientific community. The utilization of nanomaterials has become increasingly prevalent in various technological domains. The characteristics of these materials, such as their high surface area-to-volume ratio, enable their application in areas such as catalysis, energy storage, and drug delivery. It is anticipated that novel nano-photosensitizers (NPSs) will emerge as a promising avenue for scientific exploration with multifaceted and multifunctional properties. The envisioned outcome of this endeavour lies in uncovering significant and revolutionary discoveries in the field of cancer research. The concept of translating scientific discoveries from laboratory research to clinical applications, commonly referred to as bench to bedside, has thus gained significant attention in academic discourse.

Conjugated polymers are fluorescent probes with high fluorescence efficiency, remarkable photostability, and potent light absorption, among their many advantageous qualities. The potential uses of these polymers in photodynamic and photothermal therapy for the detection and treatment of cancer are being investigated. Through sophisticated chemical synthesis and flexible polymer architectures, researchers can produce new conjugated polymers with high singlet-oxygen generation capabilities for photodynamic treatment (PDT). Conjugated polymer nanoparticles that contain photosensitizers improve the formation of singlet oxygen because they transfer energy effectively. Nonetheless, there are still issues to be resolved, like reduced singlet-oxygen generation efficiency in the near-infrared (NIR) wavelength region and restrictions on light penetration. Clinical safety of the conjugated polymers is another crucial factor, along with PDT effectiveness. Any organic or inorganic nanoparticle that is ingested into the body could have negative health effects. The purpose of this article is to provide an overview of singlet oxygen generation for PDT as well as highlight the most recent developments in conjugated polymers and polymers based on nanomaterials. With an emphasis on the idea of conjugated polymers and nano-conjugated polymers as photosensitizers, we give an overview of recent discoveries for SOG in PDT research and discuss the mechanisms important to SOG and PDT cancer

therapy. In order to create singlet oxygen for photodynamic therapy, dye-based conjugated polymers have been studied as photosensitized materials. We have also mentioned the effects of dye-based conjugated polymers on singlet oxygen generation in PDT because they have not been well studied in the literature.

Author contributions

NS took the lead in conceptualization, writing and reviewing of the review article. RS contributed towards writing of the article and SSB was involved in proof-reading and reviewing of the article.

Conflicts of interest

The authors declare no competing interests.

Acknowledgements

Prof. Suryasarathi Bose would like to acknowledge DST-SERB for a Swarnajayanti fellowship. Dr Neetika Singh wishes to acknowledge the SERB-National Postdoctoral Fellowship (NPDF) (File No. PDF/2022/000556) scheme, DST, India, for providing funding to conduct this research work, and Ria Sen Gupta is grateful to MHRD for a Prime Minister's Research Fellowship (PMRF).

References

1 Y. Pang, C. Li, H. Deng and Y. Sun, *Dalton Trans.*, 2022, **51**, 16428–16438.
2 H. Li, Y. Kim, H. Jung, J. Y. Hyun and I. Shin, *Chem. Soc. Rev.*, 2022, **51**, 8957–9008.
3 P.-Y. Wu, Z.-C. Shen, J.-L. Jiang, B.-C. Zhang, W.-Z. Zhang, J.-J. Zou, J.-F. Lin, C. Li and J.-W. Shao, *Biomater. Sci.*, 2022, **10**, 6267–6281.
4 J.-O. Yoo and K.-S. Ha, *Int. Rev. Cell Mol. Biol.*, 2012, **295**, 139–174.
5 B. Lu, Y. Huang, Z. Zhang, H. Quan and Y. Yao, *Mater. Chem. Front.*, 2022, **6**, 2968–2993.
6 Q. Wang, D. K. P. Ng and P.-C. Lo, *J. Mater. Chem. B*, 2018, **6**, 3285–3296.
7 B. C. Dickinson and C. J. Chang, *Nat. Chem. Biol.*, 2011, **7**, 504–511.
8 H. Hu, J. Zhang, Y. Ding, X. Zhang, K. Xu, X. Hou and P. Wu, *Anal. Chem.*, 2017, **89**, 5101–5106.
9 K.-X. Teng, L.-Y. Niu and Q.-Z. Yang, *J. Am. Chem. Soc.*, 2023, **145**, 4081–4087.
10 N. Yesilgul, T. B. Uyar, O. Seven and E. U. Akkaya, *ACS Omega*, 2017, **2**, 1367–1371.
11 S. Jeong, W. Park, C.-S. Lee and K. Na, *Macromol. Biosci.*, 2014, **14**, 1688–1695.
12 R. A. Ponzio, L. E. Ibarra, E. E. Achilli, E. Odella, C. A. Chesta, S. R. Martínez and R. E. Palacios, *J. Photochem. Photobiol., B*, 2022, **234**, 112510.
13 M. Bregnhøj, M. Westberg, B. F. Minaev and P. R. Ogilby, *Acc. Chem. Res.*, 2017, **50**, 1920–1927.
14 P. R. Ogilby, *Acc. Chem. Res.*, 1999, **32**, 512–519.
15 J. W. Leem, S.-R. Kim, K.-H. Choi and Y. L. Kim, *Nano Convergence*, 2018, **5**, 8.
16 A. Kashyap, E. Ramasamy, V. Ramalingam and M. Pattabiraman, *Molecules*, 2021, **26**, 2673.
17 S. Bonnet, *J. Am. Chem. Soc.*, 2023, **145**, 23397–23415.
18 S. Kim, T. Tachikawa, M. Fujitsuka and T. Majima, *J. Am. Chem. Soc.*, 2014, **136**, 11707–11715.
19 A. Abdurashitov, V. Tuchin and O. Semyachkina-Glushkovskaya, *J. Innovative Opt. Health Sci.*, 2020, **13**, 2030004.
20 B. Li, L. Lin, H. Lin and B. C. Wilson, *J. Biophotonics*, 2016, **9**, 1314–1325.
21 B. Li, H. Lin, D. Chen, B. C. Wilson and Y. Gu, *J. Innovative Opt. Health Sci.*, 2013, **06**, 1330002.
22 M. Niedre, M. S. Patterson and B. C. Wilson, *Photochem. Photobiol.*, 2002, **75**, 382–391.
23 M. T. Jarvi, M. J. Niedre, M. S. Patterson and B. C. Wilson, *Photochem. Photobiol.*, 2006, **82**, 1198.
24 A. Jiménez-Banzo, X. Ragàs, P. Kapusta and S. Nonell, *Photochem. Photobiol. Sci.*, 2008, **7**, 1003–1010.
25 H.-J. Laubach, S. K. Chang, S. Lee, I. Rizvi, D. Zurakowski, S. J. Davis, C. R. Taylor and T. Hasan, *J. Biomed. Opt.*, 2008, **13**, 050504.
26 P. R. Ogilby, *Chem. Soc. Rev.*, 2010, **39**, 3181.
27 H. Lin, D. Chen, M. Wang, J. Lin, B. Li and S. Xie, *J. Opt.*, 2011, **13**, 125301.
28 J. Krajczewski, K. Rucińska, H. E. Townley and A. Kudelski, *Photodiagn. Photodyn. Ther.*, 2019, **26**, 162–178.
29 B. Song, G. Wang, M. Tan and J. Yuan, *J. Am. Chem. Soc.*, 2006, **128**, 13442–13450.
30 D. Song, S. Cho, Y. Han, Y. You and W. Nam, *Org. Lett.*, 2013, **15**, 3582–3585.
31 J. M. Aubry, B. Cazin and F. Duprat, *J. Org. Chem.*, 1989, **54**, 726–728.
32 B. Song, G. Wang and J. Yuan, *Chem. Commun.*, 2005, 3553.
33 N. Hananya, O. Green, R. Blau, R. Satchi-Fainaro and D. Shabat, *Angew. Chem., Int. Ed.*, 2017, **56**, 11793–11796.
34 H. K. Yoon, X. Lou, Y.-C. Chen, Y.-E. Koo Lee, E. Yoon and R. Kopelman, *Chem. Mater.*, 2014, **26**, 1592–1600.
35 B. A. Lindig, M. A. J. Rodgers and A. P. Schaap, *J. Am. Chem. Soc.*, 1980, **102**, 5590–5593.
36 R. Bresolí-Obach, J. Nos, M. Mora, M. L. Sagristà, R. Ruiz-González and S. Nonell, *Methods*, 2016, **109**, 64–72.
37 D. Gao, R. R. Agayan, H. Xu, M. A. Philbert and R. Kopelman, *Nano Lett.*, 2006, **6**, 2383–2386.
38 Z. Wang, X. Hong, S. Zong, C. Tang, Y. Cui and Q. Zheng, *Sci. Rep.*, 2015, **5**, 12602.

39 E. Albiter, S. Alfaro and M. A. Valenzuela, *Int. J. Photoenergy*, 2012, **2012**, 1–8.
40 E. Albiter, S. Alfaro and M. A. Valenzuela, *Photochem. Photobiol. Sci.*, 2015, **14**, 597–602.
41 M. I. Burguete, F. Galindo, R. Gavara, S. V. Luis, M. Moreno, P. Thomas and D. A. Russell, *Photochem. Photobiol. Sci.*, 2009, **8**, 37–44.
42 X.-F. Zhang and X. Li, *J. Lumin.*, 2011, **131**, 2263–2266.
43 T. Entradas, S. Waldron and M. Volk, *J. Photochem. Photobiol., B*, 2020, **204**, 111787.
44 T. Ohyashiki, M. Nunomura and T. Katoh, *Biochim. Biophys. Acta, Biomembr.*, 1999, **1421**, 131–139.
45 M. Price, J. J. Reiners, A. M. Santiago and D. Kessel, *Photochem. Photobiol.*, 2009, **85**, 1177–1181.
46 Y.-Q. He, W. Fudickar, J.-H. Tang, H. Wang, X. Li, J. Han, Z. Wang, M. Liu, Y.-W. Zhong, T. Linker and P. J. Stang, *J. Am. Chem. Soc.*, 2020, **142**, 2601–2608.
47 K. Imato, K. Ohira, M. Yamaguchi, T. Enoki and Y. Ooyama, *Mater. Chem. Front.*, 2020, **4**, 589–596.
48 E. Y. Zhou, H. J. Knox, C. Liu, W. Zhao and J. Chan, *J. Am. Chem. Soc.*, 2019, **141**, 17601–17609.
49 H. Wu, Q. Song, G. Ran, X. Lu and B. Xu, *TrAC, Trends Anal. Chem.*, 2011, **30**, 133–141.
50 K. Tanaka, T. Miura, N. Umezawa, Y. Urano, K. Kikuchi, T. Higuchi and T. Nagano, *J. Am. Chem. Soc.*, 2001, **123**, 2530–2536.
51 B. Song, G. Wang, M. Tan and J. Yuan, *J. Am. Chem. Soc.*, 2006, **128**, 13442–13450.
52 D. Zhu, D. Xing, Y. Wei, X. Li and B. Gao, *Luminescence*, 2004, **19**, 278–282.
53 Y. He, D. Xing, G. Yan and K. Ueda, *Cancer Lett.*, 2002, **182**, 141–145.
54 J. Ge, M. Lan, B. Zhou, W. Liu, L. Guo, H. Wang, Q. Jia, G. Niu, X. Huang, H. Zhou, X. Meng, P. Wang, C.-S. Lee, W. Zhang and X. Han, *Nat. Commun.*, 2014, **5**, 4596.
55 R. Vankayala, C.-L. Kuo, A. Sagadevan, P.-H. Chen, C.-S. Chiang and K. C. Hwang, *J. Mater. Chem. B*, 2013, **1**, 4379.
56 D. Bechet, P. Couleaud, C. Frochot, M.-L. Viriot, F. Guillemin and M. Barberi-Heyob, *Trends Biotechnol.*, 2008, **26**, 612–621.
57 S. J. Chadwick, D. Salah, P. M. Livesey, M. Brust and M. Volk, *J. Phys. Chem. C*, 2016, **120**, 10647–10657.
58 F. Gao, M. Sun, W. Ma, X. Wu, L. Liu, H. Kuang and C. Xu, *Adv. Mater.*, 2017, **29**, 1606864.
59 G. V. Kumari, M. A. JothiRajan and T. Mathavan, *Mater. Res. Express*, 2018, **5**, 085027.
60 R. Vankayala, C.-L. Kuo, K. Nuthalapati, C.-S. Chiang and K. C. Hwang, *Adv. Funct. Mater.*, 2015, **25**, 5934–5945.
61 H. Kawasaki, S. Kumar, G. Li, C. Zeng, D. R. Kauffman, J. Yoshimoto, Y. Iwasaki and R. Jin, *Chem. Mater.*, 2014, **26**, 2777–2788.
62 S. Miyata, H. Miyaji, H. Kawasaki, M. Yamamoto, E. Nishida, H. Takita, T. Akasaka, N. Ushijima, T. Iwanaga and T. Sugaya, *Int. J. Nanomed.*, 2017, **12**, 2703–2716.
63 M.-H. Chan, S.-P. Chen, C.-W. Chen, Y.-C. Chan, R. J. Lin, D. P. Tsai, M. Hsiao, R.-J. Chung, X. Chen and R.-S. Liu, *J. Phys. Chem. C*, 2018, **122**, 2402–2412.
64 S. Farooq and R. E. de Araujo, *Photodiagn. Photodyn. Ther.*, 2021, **35**, 102466.
65 T. Zhao, X. Shen, L. Li, Z. Guan, N. Gao, P. Yuan, S. Q. Yao, Q.-H. Xu and G. Q. Xu, *Nanoscale*, 2012, **4**, 7712.
66 C. Jiang, T. Zhao, P. Yuan, N. Gao, Y. Pan, Z. Guan, N. Zhou and Q.-H. Xu, *ACS Appl. Mater. Interfaces*, 2013, **5**, 4972–4977.
67 R. Vankayala, Y.-K. Huang, P. Kalluru, C.-S. Chiang and K. C. Hwang, *Small*, 2014, **10**, 1612–1622.
68 P. Vijayaraghavan, C.-H. Liu, R. Vankayala, C.-S. Chiang and K. C. Hwang, *Adv. Mater.*, 2014, **26**, 6689–6695.
69 M. Sakamoto, T. Tachikawa, M. Fujitsuka and T. Majima, *Langmuir*, 2009, **25**, 13888–13893.
70 T. Das, P. Ghosh, M. S. Shanavas, A. Maity, S. Mondal and P. Purkayastha, *Nanoscale*, 2012, **4**, 6018.
71 H. Saito and Y. Nosaka, *J. Phys. Chem. C*, 2014, **118**, 15656–15663.
72 N. Zhou, H. Zhu, S. Li, J. Yang, T. Zhao, Y. Li and Q.-H. Xu, *J. Phys. Chem. C*, 2018, **122**, 7824–7830.
73 C. Fang, H. Jia, S. Chang, Q. Ruan, P. Wang, T. Chen and J. Wang, *Energy Environ. Sci.*, 2014, **7**, 3431–3438.
74 G. Pasparakis, *Small*, 2013, **9**, 4130–4134.
75 Y. Yu, J. Geng, E. Y. X. Ong, V. Chellappan and Y. N. Tan, *Adv. Healthcare Mater.*, 2016, **5**, 2528–2535.
76 M. B. Rivas Aiello, J. J. Romero, S. G. Bertolotti, M. C. Gonzalez and D. O. Mártire, *J. Phys. Chem. C*, 2016, **120**, 21967–21975.
77 Z. Yuan, Z.-J. Jiang, Y. Wang, Z. Jiang and B. Deng, *J. Phys. Chem. C*, 2022, **126**, 13191–13201.
78 D. M. Willard, R. E. Riter and N. E. Levinger, *J. Am. Chem. Soc.*, 1998, **120**, 4151–4160.
79 I. Roy, T. Y. Ohulchanskyy, H. E. Pudavar, E. J. Bergey, A. R. Oseroff, J. Morgan, T. J. Dougherty and P. N. Prasad, *J. Am. Chem. Soc.*, 2003, **125**, 7860–7865.
80 M. Lal, L. Levy, K. S. Kim, G. S. He, X. Wang, Y. H. Min, S. Pakatchi and P. N. Prasad, *Chem. Mater.*, 2000, **12**, 2632–2639.
81 R. W. M. Allen, C. Templeton, M. J. Hostetler and C. T. Kraft, *J. Am. Chem. Soc.*, 1998, **120**, 1906–1911.
82 Y. Nosaka, T. Daimon, A. Y. Nosaka and Y. Murakami, *Phys. Chem. Chem. Phys.*, 2004, **6**, 2917.
83 M.-K. Tsang, G. Bai and J. Hao, *Chem. Soc. Rev.*, 2015, **44**, 1585–1607.
84 N. M. Idris, S. S. Lucky, Z. Li, K. Huang and Y. Zhang, *J. Mater. Chem. B*, 2014, **2**, 7017–7026.
85 L. Zhang, L. Zeng, Y. Pan, S. Luo, W. Ren, A. Gong, X. Ma, H. Liang, G. Lu and A. Wu, *Biomaterials*, 2015, **44**, 82–90.
86 Z. Hou, Y. Zhang, K. Deng, Y. Chen, X. Li, X. Deng, Z. Cheng, H. Lian, C. Li and J. Lin, *ACS Nano*, 2015, **9**, 2584–2599.
87 P. Kalluru, R. Vankayala, C.-S. Chiang and K. C. Hwang, *Angew. Chem., Int. Ed.*, 2013, **52**, 12332–12336.

88 Y. Xu, Z. Shi, L. Zhang, E. M. B. Brown and A. Wu, *Nanoscale*, 2016, **8**, 12715–12722.
89 D. Duan, H. Liu, Y. Xu, Y. Han, M. Xu, Z. Zhang and Z. Liu, *ACS Appl. Mater. Interfaces*, 2018, **10**, 5278–5286.
90 H. Dong, S. Tang, Y. Hao, H. Yu, W. Dai, G. Zhao, Y. Cao, H. Lu, X. Zhang and H. Ju, *ACS Appl. Mater. Interfaces*, 2016, **8**, 3107–3114.
91 H. W. Kroto, J. R. Heath, S. C. O'Brien, R. F. Curl and R. E. Smalley, *Nature*, 1985, **318**, 162–163.
92 G. A. M. Sáfar, R. N. Gontijo, C. Fantini, D. C. S. Martins, Y. M. Idemori, M. V. B. Pinheiro and K. Krambrock, *J. Phys. Chem. C*, 2015, **119**, 4344–4350.
93 D. M. Wang, M. X. Gao, P. F. Gao, H. Yang and C. Z. Huang, *J. Phys. Chem. C*, 2013, **117**, 19219–19225.
94 R. Knoblauch, A. Harvey and C. D. Geddes, *Plasmonics*, 2021, **16**, 1765–1772.
95 A. Blacha-Grzechnik, M. Krzywiecki, R. Motyka and M. Czichy, *J. Phys. Chem. C*, 2019, **123**, 25915–25924.
96 Z. M. Markovic, B. Z. Ristic, K. M. Arsikin, D. G. Klisic, L. M. Harhaji-Trajkovic, B. M. Todorovic-Markovic, D. P. Kepic, T. K. Kravic-Stevovic, S. P. Jovanovic, M. M. Milenkovic, D. D. Milivojevic, V. Z. Bumbasirevic, M. D. Dramicanin and V. S. Trajkovic, *Biomaterials*, 2012, **33**, 7084–7092.
97 W.-S. Kuo, C.-Y. Chang, H.-H. Chen, C.-L. L. Hsu, J.-Y. Wang, H.-F. Kao, L. C.-S. Chou, Y.-C. Chen, S.-J. Chen, W.-T. Chang, S.-W. Tseng, P.-C. Wu and Y.-C. Pu, *ACS Appl. Mater. Interfaces*, 2016, **8**, 30467–30474.
98 Y. Zhang, C. Yang, D. Yang, Z. Shao, Y. Hu, J. Chen, L. Yuwen, L. Weng, Z. Luo and L. Wang, *Phys. Chem. Chem. Phys.*, 2018, **20**, 17262–17267.
99 Z. Luo, D. Yang, C. Yang, X. Wu, Y. Hu, Y. Zhang, L. Yuwen, E. K. L. Yeow, L. Weng, W. Huang and L. Wang, *Appl. Surf. Sci.*, 2018, **434**, 155–162.
100 D. Zhang, L. Wen, R. Huang, H. Wang, X. Hu and D. Xing, *Biomaterials*, 2018, **153**, 14–26.
101 L.-S. Lin, Z.-X. Cong, J. Li, K.-M. Ke, S.-S. Guo, H.-H. Yang and G.-N. Chen, *J. Mater. Chem. B*, 2014, **2**, 1031.
102 C. Liu, Z. Chen, Z. Wang, W. Li, E. Ju, Z. Yan, Z. Liu, J. Ren and X. Qu, *Nanoscale*, 2016, **8**, 12570–12578.
103 L. Zhou, Y. Xu, W. Yu, X. Guo, S. Yu, J. Zhang and C. Li, *J. Mater. Chem. A*, 2016, **4**, 8000–8004.
104 M. Lismont, L. Dreesen and S. Wuttke, *Adv. Funct. Mater.*, 2017, **27**, 1606314.
105 Z. Li and Y.-W. Yang, *J. Mater. Chem. B*, 2017, **5**, 9278–9290.
106 K. Lu, C. He and W. Lin, *J. Am. Chem. Soc.*, 2014, **136**, 16712–16715.
107 K. Lu, C. He and W. Lin, *J. Am. Chem. Soc.*, 2015, **137**, 7600–7603.
108 D. Bůžek, J. Zelenka, P. Ulbrich, T. Ruml, I. Křížová, J. Lang, P. Kubát, J. Demel, K. Kirakci and K. Lang, *J. Mater. Chem. B*, 2017, **5**, 1815–1821.
109 Y. Ma, X. Li, A. Li, P. Yang, C. Zhang and B. Tang, *Angew. Chem., Int. Ed.*, 2017, **56**, 13752–13756.
110 Q. Guan, L.-L. Zhou, Y.-A. Li and Y.-B. Dong, *Inorg. Chem.*, 2018, **57**, 10137–10145.
111 F. Hu, D. Mao, Kenry, Y. Wang, W. Wu, D. Zhao, D. Kong and B. Liu, *Adv. Funct. Mater.*, 2018, **28**, 1707519.
112 T. Luo, K. Ni, A. Culbert, G. Lan, Z. Li, X. Jiang, M. Kaufmann and W. Lin, *J. Am. Chem. Soc.*, 2020, **142**, 7334–7339.
113 Y.-T. Qin, H. Peng, X.-W. He, W.-Y. Li and Y.-K. Zhang, *ACS Appl. Mater. Interfaces*, 2019, **11**, 34268–34281.
114 Y. Li, Z. Di, J. Gao, P. Cheng, C. Di, G. Zhang, B. Liu, X. Shi, L.-D. Sun, L. Li and C.-H. Yan, *J. Am. Chem. Soc.*, 2017, **139**, 13804–13810.
115 S.-Z. Ren, B. Wang, X.-H. Zhu, D. Zhu, M. Liu, S.-K. Li, Y.-S. Yang, Z.-C. Wang and H.-L. Zhu, *ACS Appl. Mater. Interfaces*, 2020, **12**, 24662–24674.
116 H. S. Jung, P. Verwilst, A. Sharma, J. Shin, J. L. Sessler and J. S. Kim, *Chem. Soc. Rev.*, 2018, **47**, 2280–2297.
117 J. Feng, W.-X. Ren, F. Kong and Y.-B. Dong, *Inorg. Chem. Front.*, 2021, **8**, 848–879.
118 T. Luo, G. T. Nash, Z. Xu, X. Jiang, J. Liu and W. Lin, *J. Am. Chem. Soc.*, 2021, **143**, 13519–13524.
119 X. Zheng, L. Wang, Q. Pei, S. He, S. Liu and Z. Xie, *Chem. Mater.*, 2017, **29**, 2374–2381.
120 L. Zhang, S. Wang, Y. Zhou, C. Wang, X. Zhang and H. Deng, *Angew. Chem., Int. Ed.*, 2019, **58**, 14213–14218.
121 S.-B. Wang, Z.-X. Chen, F. Gao, C. Zhang, M.-Z. Zou, J.-J. Ye, X. Zeng and X.-Z. Zhang, *Biomaterials*, 2020, **234**, 119772.
122 L. Yang and P. Alexandridis, *Curr. Opin. Colloid Interface Sci.*, 2000, **5**, 132–143.
123 A. Labib, V. Lenaerts, F. Chouinard, J. C. Leroux, R. Ouellet and J. E. van Lier, *Pharm. Res.*, 1991, **8**, 1027–1031.
124 E. Allémann, J. Rousseau, N. Brasseur, S. V. Kudrevich, K. Lewis and J. E. van Lier, *Int. J. Cancer*, 1996, **66**, 821–824.
125 M. J. Moreno, E. Monson, R. G. Reddy, A. Rehemtulla, B. D. Ross, M. Philbert, R. J. Schneider and R. Kopelman, *Sens. Actuators, B*, 2003, **90**, 82–89.
126 J. Fu, X. Li, D. K. P. Ng and C. Wu, *Langmuir*, 2002, **18**, 3843–3847.
127 Q. Zheng, Z. Duan, Y. Zhang, X. Huang, X. Xiong, A. Zhang, K. Chang and Q. Li, *Molecules*, 2023, **28**, 5091.
128 L. Liu, X. Wang, S. Zhu and L. Li, *ACS Appl. Bio Mater.*, 2021, **4**, 1211–1220.
129 Y. Jiang and J. McNeill, *Chem. Rev.*, 2017, **117**, 838–859.
130 C. Zhang, Q. Yuan, Z. Zhang and Y. Tang, *Molecules*, 2023, **28**, 399.
131 S. Battah, R. C. Hider, A. J. MacRobert, P. S. Dobbin and T. Zhou, *J. Med. Chem.*, 2017, **60**, 3498–3510.
132 S. Wang, F. Yuan, K. Chen, G. Chen, K. Tu, H. Wang and L.-Q. Wang, *Biomacromolecules*, 2015, **16**, 2693–2700.
133 R. M. Spada, L. P. Macor, L. I. Hernández, R. A. Ponzio, L. E. Ibarra, C. Lorente, C. A. Chesta and R. E. Palacios, *Dyes Pigm.*, 2018, **149**, 212–223.
134 S.-H. Cheng, C.-H. Lee, C.-S. Yang, F.-G. Tseng, C.-Y. Mou and L.-W. Lo, *J. Mater. Chem.*, 2009, **19**, 1252.

135 K. Chang, Y. Tang, X. Fang, S. Yin, H. Xu and C. Wu, *Biomacromolecules*, 2016, **17**, 2128–2136.
136 R. Islam, K. Kotalík, V. Šubr, S. Gao, J.-R. Zhou, K. Yokomizo, T. Etrych and J. Fang, *Nanomedicine*, 2023, **48**, 102636.
137 Y.-Q. Huang, S.-S. Jiang, L.-X. Pan, R. Zhang, K.-L. Liu, X.-F. Liu, Q.-L. Fan, L.-H. Wang and W. Huang, *New J. Chem.*, 2021, **45**, 15607–15617.
138 X. Shen, L. Li, H. Wu, S. Q. Yao and Q.-H. Xu, *Nanoscale*, 2011, **3**, 5140.
139 S. Ren, H. Li, X. Xu, H. Zhao, W. He, L. Zhang and Z. Cheng, *Biomater. Sci.*, 2023, **11**, 509–517.
140 B. Bao, X. Zhai, T. Liu, P. Su, L. Zhou, Y. Xu, B. Gu and L. Wang, *Polym. Chem.*, 2020, **11**, 7035–7041.
141 Sauraj, J. H. Kang, Oh. Lee and Y. T. Ko, *Nanoscale*, 2023, **15**, 4882–4892.
142 Z. Wang, L. Li, W. Wang, R. Wang, G. Li, H. Bian, D. Zhu and M. R. Bryce, *Dalton Trans.*, 2023, **52**, 1595–1601.
143 Z. Chen, Y. Chen, Y. Xu, X. Shi, Z. Han, Y. Bai, H. Fang, W. He and Z. Guo, *ACS Appl. Bio Mater.*, 2023, **6**, 3406–3413.
144 S. Cheng and J. Li, *Biochem. Biophys. Res. Commun.*, 2023, **652**, 55–60.
145 N. M. Vinita, U. Devan, S. Durgadevi, S. Anitha, D. Prabhu, S. Rajamanikandan, M. Govarthanan, A. Yuvaraj, M. Biruntha, A. Antony Joseph Velanganni, J. Jeyakanthan, P. A. Prakash, M. S. Mohamed Jaabir and P. Kumar, *Sci. Rep.*, 2023, **13**, 2230.
146 J. Wang, J. Wei, Y. Leng, Y. Dai, C. Xie, Z. Zhang, M. Zhu and X. Peng, *Biosensors*, 2023, **13**, 324.
147 L. Zhao, M. Chang, Z. He, Y. Zhao, J. Wang and Y. Lu, *ACS Appl. Polym. Mater.*, 2023, **5**, 1530–1538.
148 C. C. Karanlık, G. Y. Atmaca and A. Erdoğmuş, *J. Mol. Struct.*, 2023, **1274**, 134498.
149 H. Yalazan, H. Kantekin and M. Durmuş, *New J. Chem.*, 2023, **47**, 7849–7861.
150 C. Liu, Y. Wang, S. Wang, P. Xu, R. Liu, D. Han and Y. Wei, *Polymers*, 2023, **15**, 509.
151 Y. Yang, N. Li, Y. Zhu, J. Li, S. Li and X. Hou, *Talanta*, 2023, **259**, 124493.
152 R. Tan, J. Ge, C. Wang, Y. Wan and X. Yang, *Carbohydr. Polym.*, 2023, **311**, 120748.
153 N. Singh, P. Kumar, R. Kumar and U. Riaz, *Ind. Eng. Chem. Res.*, 2019, **58**, 14044–14057.
154 N. Singh, E. S. Aazam and U. Riaz, *J. Mol. Struct.*, 2021, **1240**, 130533.
155 N. Singh, S. Singh, S. M. Ashraf and U. Riaz, *Colloid Polym. Sci.*, 2020, **298**, 1443–1453.
156 N. Singh, M. Arish, P. Kumar, A. Rub and U. Riaz, *Sci. Rep.*, 2020, **10**, 57.
157 L. Zhou, F. Lv, L. Liu and S. Wang, *Acc. Chem. Res.*, 2019, **52**, 3211–3222.
158 L. Cheng, C. Wang, L. Feng, K. Yang and Z. Liu, *Chem. Rev.*, 2014, **114**, 10869–10939.
159 W. Wu, G. Feng, S. Xu and B. Liu, *Macromolecules*, 2016, **49**, 5017–5025.
160 Z. Cong, S. Xie, Z. Jiang, S. Zheng, W. Wang, W. Wang and H. Song, *Chem. Eng. J.*, 2022, **431**, 133748.
161 X. Tan, J. Wang, X. Pang, L. Liu, Q. Sun, Q. You, F. Tan and N. Li, *ACS Appl. Mater. Interfaces*, 2016, **8**, 34991–35003.
162 W. Sun, X. Wang, Z. Cheng, X. Wang, N. Fan, P. Dong, M. q. Tong, Y. Liu and W. Sun, *Biomed. Pharmacother.*, 2023, **158**, 114071.
163 M. Nave, F. J. P. Costa, C. G. Alves, R. Lima-Sousa, B. L. Melo, I. J. Correia and D. de Melo-Diogo, *Eur. J. Pharm. Biopharm.*, 2023, **184**, 7–15.
164 L. Chen, X. Li, M. Xiong, Y. Zhao, S. Liu, C. Li and K. Wang, *Mater. Des.*, 2023, **225**, 111532.
165 T. Wu, X. Lu, Z. Yu, X. Zhu, J. Zhang, L. Wang and H. Zhou, *J. Mater. Chem. B*, 2023, **11**, 1213–1221.
166 Q. Wu, Y. Zhu, X. Fang, X. Hao, L. Jiao, E. Hao and W. Zhang, *ACS Appl. Mater. Interfaces*, 2020, **12**, 47208–47219.
167 R. Peng, Y. Luo, Q. Cui, J. Wang and L. Li, *ACS Appl. Bio Mater.*, 2020, **3**, 1305–1311.

